On the specific heat capacity estimation of metal oxide–based nanofluid for energy perspective – A comprehensive assessment of data analysis techniques

Article *in* International Communications in Heat and Mass Transfer · February 2021

DOI: 10.1016/j.icheatmasstransfer.2021.105217

CITATION
1

READS
179

8 authors, including:

Mehdi Jamei
Assistant Professor, Shahid Chamran university (Technology Campus of Shohada…
26 PUBLICATIONS **96** CITATIONS
SEE PROFILE

Iman Ahmadianfar
Behbahan Khatam Alanbia University of Technology
44 PUBLICATIONS **259** CITATIONS
SEE PROFILE

Ismail Olumegbon
Elizade University
7 PUBLICATIONS **31** CITATIONS
SEE PROFILE

Contents lists available at ScienceDirect

International Communications in Heat and Mass Transfer

journal homepage: http://ees.elsevier.com

On the specific heat capacity estimation of metal oxide-based nanofluid for energy perspective – A comprehensive assessment of data analysis techniques

Mehdi Jamei[b,*], Iman Ahmadianfar[a], Ismail Adewale Olumegbon[c], Amin Asadi[d,*], Masoud Karbasi[e], Zafar Said[f], Mohsen Sharifpur[g], Josua P. Meyer[g]

[a] Dep. of Civil Engineering, Behbahan Khatam Alanbia University of Technology, Behbahan, Iran
[b] Faculty of Engineering, Shohadaye Hoveizeh University of Technology, Dasht-e Azadegan, Susangerd, Iran
[c] Dep. of Physical and Chemical Sciences, Elizade University, Ondo State, Nigeria
[d] Doral Academy of Nevada-Pebble Campus, Las Vegas, Nevada, USA
[e] Water Engineering Department, Faculty of Agriculture, University of Zanjan, Zanjan, Iran
[f] Dep. of Sustainable and Renewable Energy Engineering, University of Sharjah, P.O. Box 27272, Sharjah, United Arab Emirates
[g] Dep. of Mechanical and Aeronautical Engineering, University of Pretoria, Pretoria 0002, South Africa

ARTICLE INFO

Keywords
Nanofluids
Specific heat capacity
Metal oxide
Energy storage
Kernel extreme learning machine
Multivariate adaptive regression spline

ABSTRACT

The main aim of the present study is to investigate the capabilities of four robust machine learning method - the Kernel Extreme Learning Machine (KELM), Adaptive Regression Spline (MARS), M5 Model Tree (M5Tree), and Gene Expression Programming (GEP) model in predicting specific heat capacity (SHC) of metal oxide-based nanofluids implemented in solar energy application. Sets of 1180 data of different metal oxide-based nanofluids containing Al_2O_3, ZnO, TiO_2, SiO_2, MgO, and CuO dispersed in various base fluids were collected from reliable literature to provide the predictive model of SHC of nanofluids. The volume fraction, temperature, SHC of the base fluid, and mean diameter of nanoparticles were used as an input variable to predict nanofluids' SHC as the output variable. The artificial intelligence (AI) models were validated using several statistical performance criteria, graphical devices, and conventional models. The results obtained from all datasets demonstrated that the KELM model significantly outperformed the MARS, M5Tree, and GEP model in predicting the SHC of nanofluid. Moreover, the sensitivity analysis showed that the mean diameter of the nanoparticle and SHC of the base fluid have the most considerable impact on estimating the SHC of metal oxide-based nanofluids.

Nomenclature

C_P^{Base}
Specific heat capacity of base fluid (J/K.g)
C_P^{nf}
Specific heat capacity of nanofluid (J/K.g)
C_P^{p}
Specific heat capacity of nanoparticle (J/K.g)
C^*
Mallows Coefficient
RD
Relative deviation
D_p
Particle diameter, nm
I_A
Index of agreement
m
Mass (gr)
MAPE
Mean absolute percentage error
MSRE
Mean Square Root Error
LMI
Legates-McCabe's Index
P_c
Pearson correlation coefficient
Pr
Prandtl number
$\dot{q}$
heat transfer rate
R
Correlation coefficient

Abbreviations: CFAE, Cumulative Frequency of Absolute Relative Error; EG, Ethylene glycol; GC, Glycerol; PG, propylene glycol; RD, Relative Deviation; SHC, Specific heat capacity; W, Water.

* Corresponding authors.
E-mail addresses: M.jamei@shhut.ac.ir (M. Jamei); aminasadi64@gmail.com (A. Asadi)

https://doi.org/10.1016/j.icheatmasstransfer.2021.105217

Available online xxx
0735-1933/

Re
Reynolds number
RMSE
Root mean square error (J/K.g)
RSS
Residual sum of squares
StDev
Standard deviation
T
Temperature, (°K)

Greek

α
Thermal diffusivity (m^2/s)
ϕ
Nanoparticle volume fraction (%)
ρ_{nf}
Bulk fluid density, gr/cm3
ρ_{np}
Density of the nanoparticles, gr/cm3
ρ_{bf}
Density of the base fluid, gr/cm3
κ
Thermal conductivity (W/m.K)

Subscripts

bf
Base fluid
i
Nanoparticle ID
nf
Nanofluid
np
Nanoparticle
p
particles
ω
nanoparticle mass fraction

1. Introduction

Heat accounts for about 70 % of the total energy produced directly and indirectly [1]. Therefore, the optimization of energy consumption can be achieved with the aid of heat exchange systems. Over the years, thermal fluids have proven to be the best tool for minimizing energy loss in heat exchange systems. The search for improved heat transfer in thermal installation led to the emergence of nanofluids. Nanofluids are homogenous suspensions of nanoparticles in conventional fluids (i.e., water, ethylene glycol, oil, etc.) [2,3]. Nanofluids are characterized by upgraded thermophysical properties like thermal conductivity, specific heat capacity, viscosity, and density [3–6]. The tiny dimension and large surface area to volume proportion of the nanoparticles are responsible for enhancing the nanofluids' thermal conductive [7]. Moreover, nanofluids can navigate effortlessly in flow-channels with lower particle momentum and transmit heat at an improved rate compared to standard fluids [8]. Many researchers summarized the finding of the available literature on different aspects of nanofluids: thermophysical properties [9–11], effects of various parameters on the stability of nanofluids [12,13], different approaches to simulate the fluid flow and heat transfer of nanofluids [14–16], and applications of nanofluids [17–21]. Nanofluid has received tremendous interest from researchers over the years prompting series of findings and investigations into its unique properties and possible applications. One central area of influence is the energy-saving applications characterized by nanofluid's ability to transfer heat effectively, thereby saving energy cost and expanding the annual market size of nanofluid-based applications to an astronomical value of over 2 billion dollars [22].

Essential to nanofluids' formation is the suspended nanoparticles, which can be made of metals, non-metals, metallic-oxide, and other compounds [23]. Of all the various forms of nanofluids, metal-oxide based nanofluids are very easy to produce, chemically stable, cost less, and settles easily during production. Hence, they are preferable for use in many technological applications. Notable metal-oxide nanoparticles include CuO [24–26], Al_2O_3 [27–29], SiO_2 [30–32] and TiO_2 [30,33]. Several solar energy applications like the solar collectors featured metal-oxide based nanofluids for it helps to enhance the optical characteristics of the collector. Notable metal oxides nanofluids like Al_2O_3-water, ZnO-water, and MgO-water are used in Tubular solar collectors [34], ZnO-PG-water nanofluid is employed in DASC [35], Al_2O_3 nanofluid [36], and CuO-water nanofluid [37] are used in flat plate solar collectors. Some of the most common applications of metal oxide-based nanofluids in energy systems are depicted in Fig. 1.

Many researchers have examined the SHC of various nanofluids and evaluated the factors affecting it. The nanofluid's SHC depended on many physicochemical properties like nanoparticle dimension, volume fraction, and SHC. Besides, the base fluid SHC, temperature, and type can affect the SHC of the nanofluid [38]. Some of the experimental research on metal-oxide based nanofluids' SHC are presented in Table 1.

In as much as empirical models have offered an alternative to experimental investigation with regards to the quantitative determination SHC of nanofluid, their accuracy has been affected by several underlying factors such as the theoretical assumptions governing the relationship between the variables, specificity, and incomplete description of

Fig. 1. Different applications of metal-oxide based nanofluids in energy systems.

Table 1
Experimental investigation of metal-oxide based nanofluids Specific heat capacity (SHC).

Nanofluids	Base fluid	Studied factors	Equipment	Reference
Al_2O_3	Water- EG	Nanoparticle volume fraction, temperature	Micro DSC II micro-calorimeter	Barbes et al. [38]
CuO	Water-EG	Nanoparticle volume fraction, temperature	Micro DSC II micro-calorimeter	Barbes et al. [39]
Al_2O_3, ZnO, SnO	Water-EG, water	Nanoparticle volume fraction, temperature	Unspecified	Vajjha et al. [40]
Al_2O_3	Water-EG	Nanoparticle volume fraction, temperature	Differential scanning calorimeter (DSC)	Elias et al. [41]
TiO_2, Al_2O_3	DI-water, EG, Engine-oil	Nanoparticle volume fraction and type, base fluid type	Double-hot wire technique	Murshed et al. [42]
Al_2O_3	Water	Nanoparticle volume fraction	Differential scanning calorimeter (DSC)	Zhou et al. [43]
Metal oxides	Poly-a olefin, mineral oil, EG, W-EG, and calcium nitrate tetrahydrate	Nanoparticle mass fraction, the heat capacity of the base fluid	Differential scanning calorimeter (DSC)	Starace et al. [44]
TiO_2, Al_2O_3	Water, EG	Nanoparticle concentration, temperature	Differential scanning calorimeter (DSC)	Nieh et al. [30]
Al_2O_3	Water	Nanoparticle volume fraction, temperature	Differential scanning calorimeter (DSC)	Heyhat et al. [45]
Al_2O_3, CuO, SiO_2	PG-W(60:40)	Nanoparticle volume fraction, temperature	Differential scanning calorimeter (DSC)	Hanley et al. [46]
SiO_2	EG, EG-GC, and EG-GC	Nanoparticle volume fraction	differential scanning calorimeter (DSC1, Mettler-Toledo)	Akilu et al. [47]

the anomalous nature of nanofluids. Given those mentioned above, computational intelligence techniques such as machine learning (ML) methodologies are employed because they offer a better estimate with a higher degree of accuracy [48–50]. Over the years, ML models have successfully predicted several nanofluid thermo-physical properties like viscosity [4], thermal conductivity [51], and even SHC [52–54] by modeling experimental data using artificial neural networks (ANN) [55] and support vector regression (SVR). In general, ML model design for nanofluids involves the training of experimental data with its physical, chemical, and environmental properties as input features and the thermophysical property as the target variable so that the ML algorithm of choice can capture the patterns in the data and establish a model structure that can be tested with another group of a dataset to predict a particular thermophysical property [56–58]. Alade et. al. [53] was the first to develop an ML model that predicted the SHC of metal-oxide based nanofluids. They used hybrid Genetic algorithm-Support vector regression in estimating the SHC of Al_2O_3/water nanofluid. Besides, machine learning models have been deployed to estimate the SHC of metal oxide-based nanofluids. Such studies include the application of SVR-based techniques for predicting SHC of CuO-based nanofluids [59,60], Al_2O_3-based nanofluids [53,60,61], SiO_2 -based nanofluids [61], and TiO_2-based nanofluids [61]. Moreover, Jamei et al. [62] provided an accurate Gaussian process regression (GPR) model for the prediction of the SHC of nanofluids. Recently, the multivariate adaptive regression spline (MARS) gave a successful estimation of the thermal conductivity of metal oxide-based nanofluids [63] and dynamic viscosity [64] of nanofluids. Just recently, the M5 model tree (M5Tree) was used to model the dynamic viscosity [65], thermal conductivity [58], and predict the Nusselt number and output temperature of CuO based nanofluid [66]. Similarly, Gene expression programming (GEP) was used to estimate the viscosity of Newtonian nanofluids [58] and predict the thermal conductivity of CuO and Al_2O_3 based nanofluids [67]. None of these four machine-learning methodologies has been utilized for modeling and estimating the SHC of nanofluids to the best of our knowledge. In this study, the Kernel extreme learning machine (KELM) technique, as the main novelty of the current study, was implemented compared to the MARS, M5Tree, and GEP to predict the SHC of metal oxide-based nanofluids. Various statistical performances, Graphical tools, and physical trend examinations were utilized to validate and evaluate the AI models. Furthermore, a qualitative response assessment, robustness measurement, and a comprehensive sensitivity analysis were carried out for SHC of metal oxide nanofluids predictive models.

2. Empirical Model of SHC and background

Specific heat capacity (SHC) of nanofluids can be described as a measure of the nanofluid's heat retentive property. Hence, it defines the thermal behavior of the nanofluid. Moreover, the heat capacity measurement can facilitate the determination of other thermal related quantities such as the thermal diffusivity, total heat transfer rate, heat exchanger effectiveness, and Nusselt number [38,47,68–72] as shown in the governing equations 1 - 4. Furthermore, the SHC is a critical parameter necessary for the accurate design and assembly of heat management applications and heat transfer systems to reduce energy loss and maximize energy conservation [73]. Hence, it is crucial that the SHC is accurately determined to ensure that the parameters in equations 1 – 4, which depend on the SHC, are correctly obtained. The following equations 1 – 4 express the dependence between thermal related quantities of thermal diffusivity, total heat transfer, heat exchange effectiveness, Nusselt number, and the specific heat capacity as:

$$\alpha = \frac{\kappa}{\rho C_p} \tag{1}$$

α, κ, ρ, C_p are thermal diffusivity, thermal conductivity, density, and specific heat capacity, respectively.

$$\dot{q} = \dot{m} C_p \Delta T \tag{2}$$

$\dot{q}, \dot{m}, \Delta T$ are total heat transfer rate, fluid mass flow rate, and temperature change, respectively.

$$\varepsilon = \frac{1-e^{(-NTU.(1-C^*))}}{1-C^* e^{(N-TU(1-C^*))}}, \quad C^* = \frac{C_{\min}}{C_{\max}}, C = \dot{m} C_p, \text{and } NTU = \frac{UA}{C_{\min}} \tag{3}$$

C^*, C_{min}, C_{max}, ε, *NTU*, *U*, and *A* are heat capacity ratio, the minimum heat capacity rates, the maximum heat capacity rates, heat exchanger effectiveness, number of transfer units, overall heat transfer coefficient, and heat transfer surface area, respectively.

$$Nu = 0.023 * \mathrm{Re}^{0.8} * \mathrm{Pr}^{0.4}, \quad \mathrm{Pr} = \frac{C_p \mu}{k} \tag{4}$$

Nu and Pr are Nuselt number and Prandtl number, respectively.

Based on the number of factors capable of varying the SHC of nanofluids, conducting experimental findings can be laborious if we have to consider individual factors or a combination of factors, thereby creating an unwanted delay in measuring SHC [74]. Moreover, the high cost of materials and experimental set-up for nanofluids experiment can cause delays to the rapid quantification of the specific heat capacity [75]. Researchers have developed empirical models as an alternative to experimental investigations in the face of inadequate experimental resources. These models are based on the theoretical understanding of nanofluids' SHC and its dependence on the factors that govern their behavior. There are two main proposed theoretical models based on the mixing theory for ideal gas mixtures and the first law of thermodynamics. Hence, they are described as the mixing rule model [76] and the thermal equilibrium model [77] (also known as model 1 and model 2, respectively) [78–80]. They are the two notable models that have estimated nanofluids' specific heat capacity with a high degree of accuracy. The mixing model, which was proposed by Pak and Cho [78] as a result of unavailable experimental data, established a relationship between the SHC of nanofluid, nanoparticles, and base fluid is expressed as follows [76,78]:

$$C_{P\,1}^{nf} = \phi C_P^{np} + (1-\phi)\, C_P^{Base} \tag{5}$$

where ϕ, $C_P{}^{nf}$, $C_P{}^{np}$, and $C_P{}^{Base}$ represent the nanoparticle volume fraction, SHC of nanofluid, SHC of nanoparticles, and SHC of the base fluid, respectively. The nanoparticle volume fraction can be converted to the corresponding mass fraction using $\phi = \frac{w}{w+(\rho_{np}/\rho_{bf})(1-w)}$. However, the limitation of model 1, despite its huge success, is its inability to account for nanofluids' SHC with large nanofluid/base fluid density differences. For a better capture of the experiment conditions, model 2, based on the thermal equilibrium between nanoparticles and the base fluid, can also be written in terms of densities and volume fraction in the form of model (II) as follows [77–79].

$$\begin{aligned} C_{P\,2}^{nf} &= \frac{\varphi\rho_{np}C_P^{np} + (1-\varphi)\,\rho_{bf}C_P^{Base}}{\varphi C_P^{np} + (1-\varphi)\,\rho_{bf}}, \rho_{nf} \\ &= (1-\phi)\,\rho_{bf} + \phi\rho_{np} \end{aligned} \tag{6}$$

where ρ_{nf}, ρ_{np}, ρ_{bf} represent the bulk fluid density, nanoparticle density, and base fluid density, respectively. Subsequently, in what was termed model 3, the isobaric specific heat capacity of nanofluid was estimated as a function of the nanoparticle mass concentration w with the relation below in (7).

$$C_{P\,3}^{nf} = wC_p^p + (1-w)\, C_p^{Base} \tag{7}$$

Over the years, these theoretical models have been used to calculate the SHC of common metal-oxide based nanofluids such as Al_2O_3 [80], MgO, ZnO, and SrO_2 dispersed in ethylene glycol (EG)-water [81] and so on. A highlight of some regression-based correlations (models) for estimating the SHC of metal oxide-based nanofluids is presented in Table 2 below. In many of these research studies, model II showed high accuracy compared to model I and gave poorly accurate SHC values for other nanofluids [74,75,82].

Table 2
Highlight of some published works on regression-based correlations (models) for estimating the SHC of metal oxide-based nanofluids.

Metal oxide based nanofluid	Theoretical model/correlations	Remarks	Reference
Al_2O_3/water, T_iO2/water	$C_P{}^{nf} = \phi C_P{}^{np} + (1-\phi)C_P{}^{Base}$	SHC decreases with an increase in nanoparticle volume concentration	Pak and Cho [78]
Al_2O_3/EG-water, ZnO/EG-water, SiO_2/deionized water	$\frac{C_P^{nf}}{C_P^{Base}} = \frac{\left[(A\times T)+\left(B\times\frac{C_P^{np}}{C_P^{Base}}\right)\right]}{C+\phi}$ A, B, C are curve fit coefficient	SHC decreases with an increase in nanoparticle volume concentration and decrease in temperature	Vajjha and Das [83]
CuO/EG	$C_P^{nf} = \frac{\varphi\rho_{np}C_P^{np}+(1-\varphi)\rho_{bf}C_P^{Base}}{\varphi C_P^{np}+(1-\varphi)\rho_{bf}}$	SHC decreases with an increase in nanoparticle volume concentration	Zhou et al. [84]
SiO_2/$LiCO_3$-K_2CO_3	$C_P^{nf} = \frac{\rho_{np}\phi_{np}C_P^{np}+\rho_{bf}\phi_{bf}C_P^{Base}}{\rho_{np}\phi_{np}+\rho_{bf}\phi_{bf}}$	The addition of SiO_2 nanoparticles at 1% mass conc. increases the SHC of the base fluid by 14.5%	Shin and Banerjee [31]

Table 3
Details of the employed experimental data points for designing the predictive SHC models.

References	Number of data	Nanoparticle	Base fluid
[45,85–92]	501	Al_2O_3	Water, EG, EG-Water (40:60), R134a, PG-W(60:40)
[92–94]	260	CuO	Water, EG, PG-W(60:-40), DW
[86,87,95]	165	SiO_2	Water, EG, GC, EG-GC
[33,87,92]	46	TiO_2	Water, PG-W(60:-40)
[86,92]	167	ZnO	EG-Water (40:60), PG-W(60:40)
[96,97]	41	MgO	Water, EG-DW

3. Dataset description and best feature selection procedure

In the first step of providing a data-driven model, the predictive models' reliability and adaptability are dependent on the integrity of the implemented database, which refers to its completeness, accuracy, and consistency of data. In this research, 1,180 reliable experimental data points were collected from 12 references to design the data-driven models for predicting SHC of a wide variety of metal oxide-based nanofluids. The collected data implemented in the design of these predictive AI-based models are listed in Table 3.

Selecting the optimal influential variables (or independent parameters) subset among all existing useful parameters has always been one of the most challenging issues in the preprocessing stage of providing predictive AI-based models. It should be carefully considered [98]. The feature selection procedure plays a vital role in the model's potential improvement and computational efficiency by decreasing the number of features. The best subsets regression algorithm is an efficient approach for indicating the optimum independent variables based on the best subsets regression fits all possible models. In this process, three criteria, namely, adjusted R-squared, Mallows (C^*), and standard error (S) are usually employed for picking the best fitting models [99]. The Mallow coefficient relationship is defined based on the residual sum of squares (RSS_k) for the regression model using k features and mean squared error (MSE_m(for the model with all existing feature as follows [99]:

$$C^* = \frac{RSS_k}{MSE_m} + 2k - N, m>k \tag{8}$$

According to Table 4, the regression analysis of various influential input combinations was assessed where N denotes the number of data points. It showed that the combination comprising of the entire input variables (Combo 11) with the highest (R^2=, 82.2%, and R^2-adj =82.1%) and lowest value of Mallow's coefficient and standard error (C^*=7, S=0.29) was identified as the optimum selection for providing the predictive model.

The influential independent variables of the optimum combination include the solid volume fraction (ϕ), temperature (T), mean diameter of nanoparticle (D_p), and SHC of nanoparticle ($C_P{}^p$), SHC of base fluid ($C_P{}^{Base}$), and density of nanoparticle (ρ_p), whereas the heat capacity (SHC) of metal oxide-based nanofluids is defined as the target. Thus, the relationship between all predictors and target ($C_P{}^{nf}$) can be defined as follows:

$$C_P^{nf} = f\left(\phi, T, C_P^p, C_P^{Base}, D_p, \rho_p\right) \tag{9}$$

where $\varphi = (m/\rho)_{np}/((m/\rho)_{np} + (m/\rho)_{bf})$ and m is the mass of the nanoparticle. In this study, the data set was randomly divided into two sections: 75% (885 data points) and 25% (295 data points) of data points, which were used to perform training and testing stages, respectively. Table 5 addresses the descriptive statistics, Pearson correlation coefficient of all input variables with the SHC of metal oxide-based nanofluids, and the normality criteria of all the data using the Anderson-Darling test [100]. According to Table 5, despite the small value of skewness and kurtosis of variables, the Anderson-Darling normality test demonstrated that none followed the Gaussian distribution. Although, the temperature having the minimum value of estimated distance (A_2=7.932) from the Anderson-Darling test is the nearest parameter to the Gaussian distribution among all predictors. Moreover, the Pearson correlation coefficient of input parameters with the target shows the SHC of base fluid has the most linear correlation (P_c =0.79) with SHC of metal oxide-based nanofluids (Fig. 2).

Furthermore, the independent variables and the response are scaled and normalized between 0 and 1 to reduce computational cost and complexity of predicting procedure using the below equation:

$$x_{nor} = \frac{x - x_{\min}}{x_{\max} - x_{\min}} \tag{10}$$

where the normalized value of datasets is defined with x_{nor} is the value, x is the original value of the dataset, x_{max} and x_{min} are the maximum and minimum of the entire dataset implemented in providing the predictive models, respectively.

4. Methodology

4.1. M5Tree model

M5Tree model initially proposed by Quinlan [101], and its structure is based on binary decision trees. In recent years, the M5Tree model has made significant progress in classification and regression problems [66,102,103]. A decision tree usually consists of four parts: roots, branches, nodes, and leaves. The tree model is the development, idea, and concept of classification and regression trees with an inverted tree structure that includes a root node at the top of the tree, which branches off to other nodes and leaves, in a dramatic manner and in the form of if-then rules. This model can extract knowledge in the form of mathematical relations from the data set.

The idea behind this model is that it analyzes a multivariate modeling problem by dividing it into smaller sub-problems and combining the results. For this purpose, the problem space is divided into subdomains, and for each subdomain, a multivariate linear regression model is fitted. With this method, we will have a set of models; each of them

Table 4
Best subsets regression results for determining the optimum input combination

Combo	Vars	R^2 (%)	R^2-adj (%)	Mallows- C^*	S	φ	T	$C_P{}^p$	$C_P{}^{Base}$	D_P	ρ_p
1	1	61.7	61.7	1012.3	0.42				X		
2	1	11.5	11.4	3496.2	0.64		X				
3	2	69.7	69.7	618.1	0.37				X	X	
4	2	66.9	66.8	759.5	0.39				X		X
5	3	72.9	72.8	464.1	0.35		X		X	X	
6	3	72.9	72.8	465.3	0.35	X			X		X
7	4	76.4	76.3	292.6	0.33	X			X	X	X
8	4	75.7	75.6	325	0.34	X		X	X		X
9	5	80.1	79.9	113.4	0.30	X		X	X	X	X
10	5	78.9	78.8	169.9	0.31	X	X		X	X	X
11	**6**	**82.2**	**82.1**	**7**	**0.29**	**X**	**X**	**X**	**X**	**X**	**X**

Table 5
The descriptive statistics of predictive variables and targets.

Statistics	φ(%)	T(K)	$C_P{}^p$(J/K.g)	$C_P{}^{Base}$(J/K.g)	D_P(nm)	ρ_p(gr/cm ^{3})	$C_P{}^{nf}$(J/K.g)
Mean	3.8184	322.01	0.69414	3.3985	40.818	4.3594	3.0246
StDev	2.883	24.03	0.12398	0.5876	17.554	1.4579	0.6762
Coef.Var	75.5	7.46	17.86	17.29	43.01	33.44	22.36
Minimum	0	241.82	0.514	1.3707	13	2.22	1.0434
Maximum	10	364.13	0.896	4.195	77	6.5	4.2875
Skewness	0.66	-0.87	-0.27	-0.36	0.78	0.28	0.22
Kurtosis	-0.65	1.33	-1.37	-0.42	0.02	-1.22	-1.12
Pearson Coef. with $C_P{}^{nf}$	-0.088	0.33	0.099	0.79	-0.229	-0.188	1.00
A_2: Anderson-Darling test	24.11	7.932	50.91	23.12	46.32	63.18	22.28
P value	<0.0001	<0.0001	<0.0001	<0.0001	<0.0001	<0.0001	<0.0001

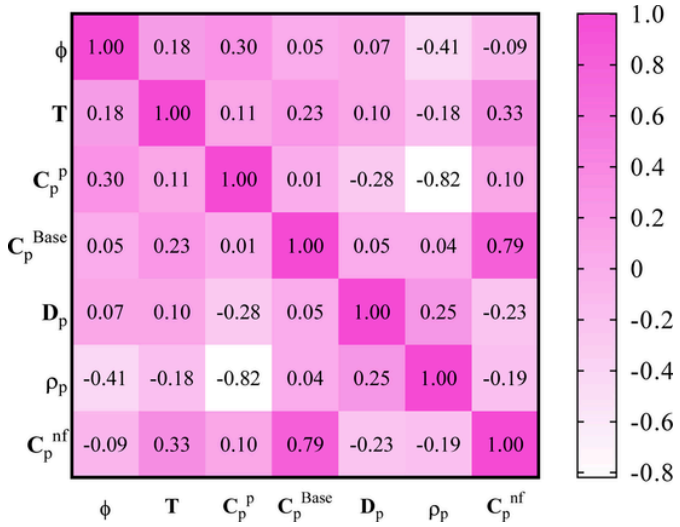

Fig. 2. The Pearson correlation coefficient between the independent input variable and C_p^{nf}

is only valid for a part of the problem domain [104]. Therefore, a piecewise linear regression model is formulated to approximate the relationship between input and output variables. This algorithm performs possible separations in multivariate space and automatically creates models for these domains. We have a sort tree with the separation of rules in internal nodes and its output in leaves. The tree model is the method of dividing and overcoming traits for samples that reach a node. First, the tree model creates a regression tree by dividing the problem space backward. In this algorithm, the standard deviation parameter of the target variable values is used as a measurement error in that node to create a branch in a division node. A test is performed to perform the division operation in the said node. Then, an attribute that further reduces the deviation. Fig. 3 shows a schematic of how the input data input is divided by the M5 tree model.

The criterion is selected as the attribute to be branched. The standard deviation reduction calculation (SDR) equation is as follows [105]:

$$\mathrm{SDR} = \mathrm{StDev}\,(\mathrm{D}) - \sum_{i=1}^{N} \frac{|T_i|}{|T|}\mathrm{StDev}\,(T_i) \tag{11}$$

$$\mathrm{StDev}\,(T) = \sqrt{\frac{1}{N}\left(\sum_{i=1}^{N} y_i^2 - \frac{1}{N}\left(\sum_{i=1}^{N} y_i\right)^2\right)} \tag{12}$$

T in relation (11) contains samples that have reached the node. T_i are sets that are obtained by dividing the node by the selected attribute, StDev is the standard deviation, y_i is the target value and N is the total number of data.

Model M5Tree is a tree model for predicting continuous numerical traits in which linear regression functions appear on this tree's leaves. The branching process is repeated many times in each node to reach the final node (leaf) wherein the leaf, the (SSD) sum of the squared deviations from the mean of the data is approximately zero. Through this process, a large tree will be developed. Working with this large tree would be difficult, so to achieve an optimal and efficient tree, a pruning process is required to eliminate additional branches. Two different pruning approaches are 1) Pruning before forming the maximum tree 2) Pruning after forming the maximum tree. In the first approach, the production of additional branches is allowed by pruning action. Still, in the second approach, pruning is performed after the maximum tree formation. By minimizing the prediction error, the optimal tree is achieved. After pruning, the smoothing process is performed to compensate for sharp ruptures that inevitably occur between adjacent linear models on pruned tree leaves, especially for models made from smaller amounts of samples [105].

4.2. Multivariate adaptive regression spline (MARS)

Multivariate Adaptive Regression Spline (MARS), as a non-parametric regression approach, was introduced by Friedman (1991) [106]. The MARS model consisted of a collection of simple linear models that spontaneously recognize trends (or patterns) related to nonlinearities and interactions among the specific problem's parameters. This technique is developed within the forward and backward stepwise stages. In the forward stage, after processing several splits, a complicated and over parametrized model is obtained in which the accuracy level of the specific model decreases [107]. Afterwards, the backward stepwise stage begins with eliminating the arbitrary input variables among the datasets that have been selected previously. The mathematical equation in the MARS model is expressed as:

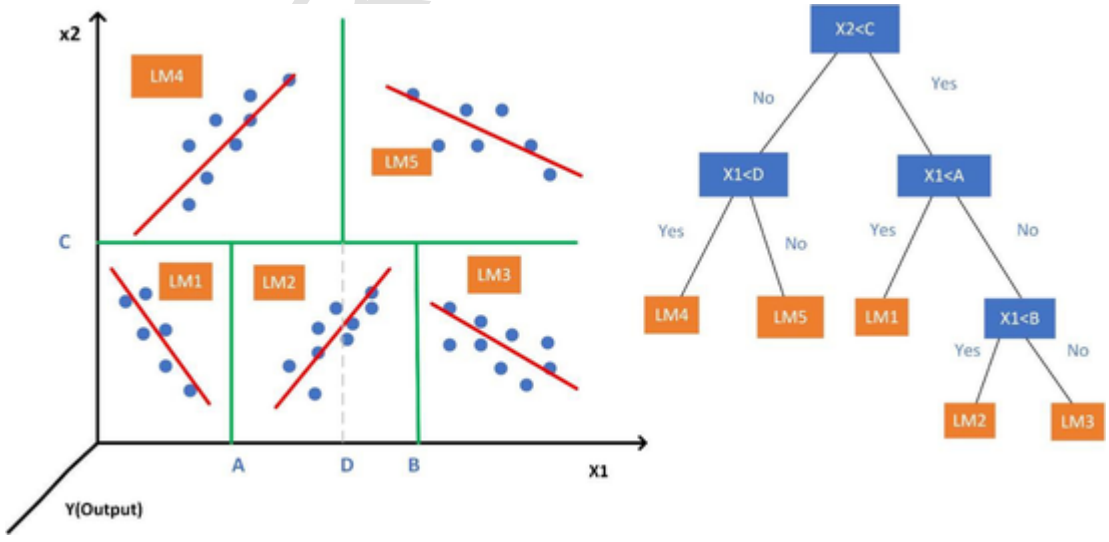

Fig. 3. Schematic view of input space division by the M5Tree and model generation

$$Y = f(x) = \beta_0 + \sum_{i=1}^{N^*} \beta_i B_{F,i}(x) \tag{13}$$

where Y denotes the target parameter, $B_{F,i}$ denotes the basis functions with the piecewise linear, β_0, β_i, and N^* denote the constant term (so-called 'knot'), basis functions (BFs) coefficient, and number of BFs, respectively [108,109]. The coefficients are introduced as weights, which demonstrate the relative significance of each input variable. The basis functions are principally described in the following [110]:

$$B_{F,i}^{-} = -(Y - h_i)_+ = \begin{cases} -(Y - h_i) & Y < h_i \\ 0 & otherwise \end{cases} \tag{14}$$

$$BF_i^{+} = (Y - h_i)_+ = \begin{cases} Y - h_i & Y > h_i \\ 0 & otherwise \end{cases} \tag{15}$$

where $B_{F,i}^{+}$ and $B_{F,i}^{-}$ are indicative of the positive and non-positive sections of spline functions, respectively, and h_i indicates the knot of the spline (threshold value). Similarly, in the process of the backward stepwise stage, some of the BFs, created among the previous process might be redundant. These BFs were removed through the Generalized Cross-Validation (GCV) criterion until the 'lack of fit' criterion is a minimum predicting precision improvement [111]. The GCV formula is expressed as [110,112] :

$$GCV = \frac{\sum_{j=1}^{ND}\left(Z_i - \hat{Z}_i\right)^2}{ND\left(1 - \frac{NB + 0.5d(NB-1)}{ND}\right)^2} \tag{16}$$

where Z_i is the observed value of output (or independent variable) of i^{th}; $\hat{Z}_i$ is the value estimated by MARS; *ND* is the number of observations; *NB* is the number of BFs and *d* denotes penalty value for each BF.

4.3. Gene expression programming (GEP)

GEP is a learning method to develop mathematical modeling, proposed by Ferreira [113]. It is a type of evolutionary computation and is based on the concept of natural evolution. The GEP is like genetic programming (GP), with the difference that it utilizes fixed-length string (chromosome) for program modeling, which is then described as expression trees (ETs). In general, GEP is made up of two parts: chromosomes and expression trees. Chromosomes are composed of a set of genes, and a gene contains two parts: the head and the tail. A head can be made by mathematical functions (−, +, /, ×) and terminal symbols (*x*, *y*, *z*, -2), and a tail is comprised of terminal symbols [114,115]. GEP starts with a set of random solutions represented by chromosomes. After that, the chromosomes are drawn in the ET form and assessed in regard to an objective function and chosen based fitness to regenerate using genetic operators (crossover and mutation). The new solutions go through the same procedure until the stopping criteria are met. The flowchart of the GEP method is displayed in Fig. 4.

4.4. Extreme learning method (KELM)

Huang et al. [116] introduced the ELM for SLFNs (single layer feed-forward neural networks) with randomly selected input weights and hidden nodes and analytically defined output weights. It possesses an outstanding generalization ability. For generalized SLFNs, the ELM output function is:

$$\begin{aligned} f_L(x) &= \sum_{i=1}^{L} \beta_i h_i(x_j) \\ &= \sum_{i=1}^{L} \beta_i h(w_i . x_j + b_i) \\ &= h(x)\beta \\ &= T_i \quad j \\ &= 1, \ldots, N \end{aligned} \tag{17}$$

where w_i is the weight vector which makes a connection between the input nodes and i^{th} hidden node, b_i is the bias of *i*th hidden node, β_i is the weight which connects i^{th} hidden node to the output node, T_j is target vector, $h(.)$ is activation function, and $f_L(x)$ represents the output of the SLFSN. Equation (8) can be written following as:

$$H\beta = T \tag{18}$$

It is possible to obtain the smallest training error by calculating the corresponding least-squares solution:

$$\beta = H^{\dagger} T \tag{19}$$

where $H^{\dagger}$ is the inverse of the generalized MP (Moore-Penrose) matrix and when HH^T*is* non-singular, it can be solved as:

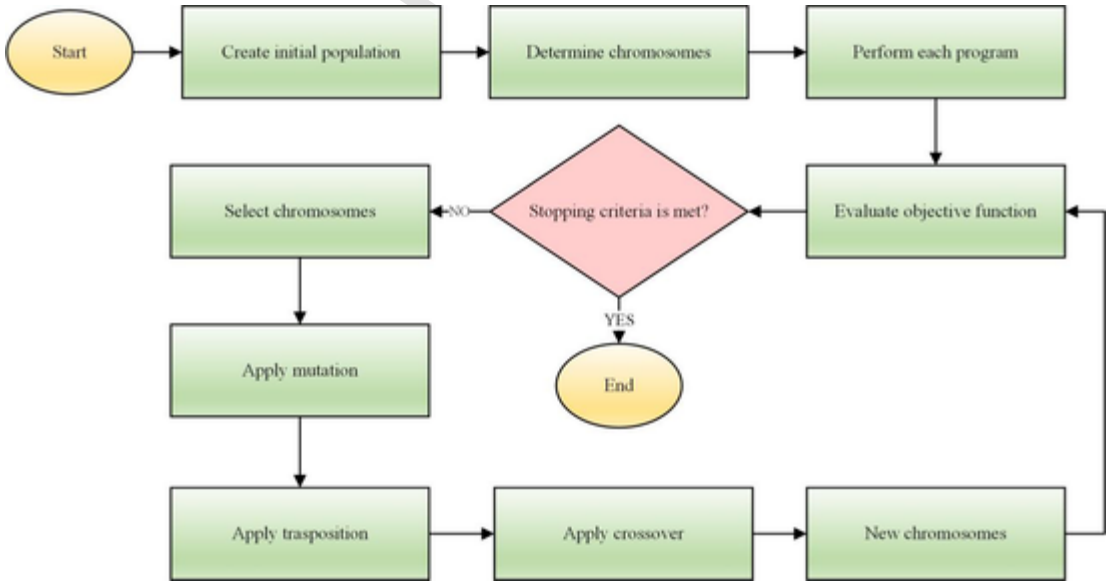

Fig. 4. Flowchart of GEP method.

$$H^{\dagger} = H^{T}\left(HH^{T}\right)^{-1} \tag{20}$$

and finally, the output function of ELM comes as follows:

$$f(x) = h(x).\beta = h(x)\left(H^{T}H + \frac{I}{C}\right)H^{T}T \tag{21}$$

where C is the regularization coefficient for optimization and I denotes the identity matrix.

If the activation function in the ELM method is replaced by a kernel function, the kernel extreme learning machine (KELM) method is written as follows [116]:

$$\Omega = HH^{T} \;:\; \Omega_{ELM\,i,j} = h(x_i)\,h(x_j) = K(x_i, x_j) \tag{22}$$

The output of the KELM function is expressed as follows:

$$f(x) = \begin{bmatrix} K(x, x_1) \\ \vdots \\ K(x, x_N) \end{bmatrix}\left(\Omega_{ELM} + \frac{I}{C}\right)^{-1} T \tag{23}$$

This approach involves specifying the kernel function and its parameters and eliminating the activation function and the number of hidden layer nodes. Different kinds of kernel functions can be used in this KELM model, such as RBF, linear, polynomial, and wavelet kernels. Among the mentioned kernels, the RBF kernel has been one of the most common kernels used in various researches [117,118]. As a result, we used the RBF kernel in the present study. The RBF kernel function is defined as follows.

$$k(x_i, x_j) = \exp\left(-x_i - x_j^{2}\right)/2\sigma^{2} \tag{24}$$

where σ represents the kernel width RBF, the KELM structure is shown in Fig. 5.

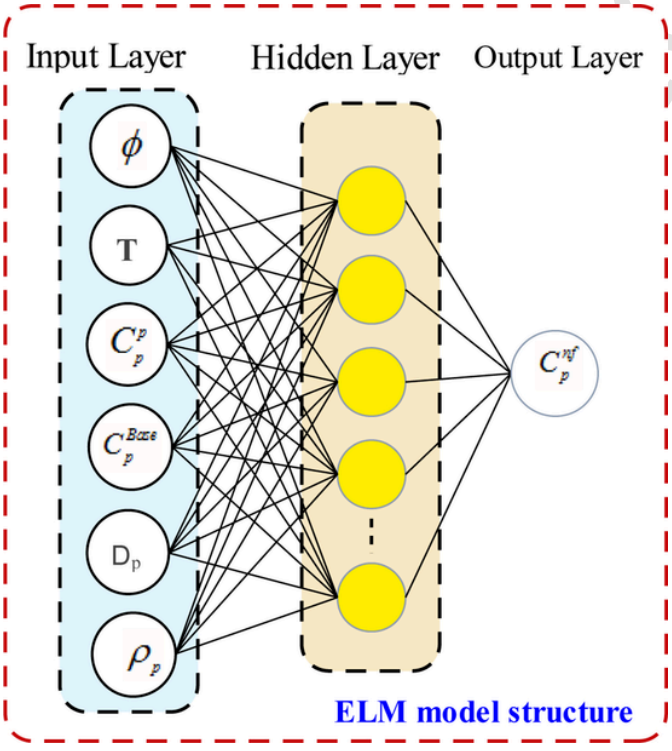

Fig. 5. Six inputs, hidden layers, and one output KELM structure.

5. Performance assessment

Various statistical criteria are employed to quantitatively evaluate the robustness and efficiency of the predictive power of AI-based models. These criteria include the Correlation Coefficient (R), Root Mean Squared Error (RMSE), Mean Absolute Percentage Error (MAPE), and Mean Square Root Error (MSRE). Besides, Legates-McCabe's Index (LMI) and Willmott's Index of agreement (I_A) [119] as the normalized goodness-of-fit metrics and are all implemented in this study for better validation.

$$R = \frac{\sum_{i=1}^{N}\left(C_{P\,c,i}^{nf} - \overline{C}_{P\,c}^{nf}\right)\cdot\left(C_{P\,o,i}^{nf} - \overline{C}_{P\,o}^{nf}\right)}{\sqrt{\sum_{i=1}^{N}\left(C_{P\,c,i}^{nf} - \overline{C}_{P\,c}^{nf}\right)^{2}\sum_{i=1}^{N}\left(C_{P\,o,i}^{nf} - \overline{C}_{P\,o}^{nf}\right)^{2}}}, \quad 0 < R \le 1 \tag{25}$$

$$RMSE = \left(\frac{1}{N}\sum_{i=1}^{N}\left(C_{P\,o,i}^{nf} - C_{P\,c,i}^{nf}\right)^{2}\right)^{0.5} \tag{26}$$

$$MAPE = \frac{1}{N}\sum_{i=1}^{N}\frac{\left|C_{P\,o,i}^{nf} - C_{P\,c,i}^{nf}\right|}{C_{P\,o,i}^{nf}} \tag{27}$$

$$LMI = 1 - \frac{\sum_{i=1}^{N}\left|C_{P\,o,i}^{nf} - C_{P\,c,i}^{nf}\right|}{\sum_{i=1}^{N}\left|C_{P\,o,i}^{nf} - \overline{C}_{P\,o}^{nf}\right|}, \quad 0 < LMI \le 1 \tag{28}$$

$$MSRE = \frac{1}{N}\sum_{i=1}^{N}\left(\frac{C_{P\,o,i}^{nf} - C_{P\,c,i}^{nf}}{C_{P\,o,i}^{nf}}\right)^{2} \tag{29}$$

$$I_A = 1 - \frac{\sum_{i}^{N}\left(C_{P\,o,i}^{nf} - C_{P\,c,i}^{nf}\right)^{2}}{\sum_{i=1}^{N}\left(\left|\left(C_{P\,o,i}^{nf} - \overline{C}_{P\,o}^{nf}\right)\right| + \left|\left(C_{P\,o,i}^{nf} - \overline{C}_{P\,o}^{nf}\right)\right|\right)^{2}}, \quad 0 < I_A \le 1 \tag{30}$$

where $C_P^{nf}{}_{c,i}$ and $C_P^{nf}{}_{o,i}$ denote the predicted and observed SHC of metal oxide-based nanofluids, respectively. Also, $\overline{C_{Pc}}$ and $\overline{C_{Po}}$ are mean values of predicted and observed SHC of metal oxide-based nanofluids. N is the number of data points. The accuracy of the predictive model is enhanced if the NRMSE and MAPE close to zero. R, *LMI*, and I_A closed to unity demonstrate the model's better performance. Besides, various graphic criteria have been used to express each of the provided models' capabilities, making it easier to judge the choice of the superior model. These tools comprise of the scatter plots and error distribution plots.

6. Models configuration and development

As mentioned in the literature, the SHC of metal oxide-based nanofluids is one of the most significant thermo-physical properties whose precise estimation plays a substantial role in analyzing the current commercial thermal energy storage system [120]. In this research, four robust ML approaches (i.e., KELM, MARS, M5Tree, and GEP models) have been applied to accurately predict the SHC of metal oxide-based nanofluids. Fig. 6 depicts the road map for estimating the SHC of metal oxide-based nanofluids using KELM, GEP, MARS, and M5Tree models.

Six input variables fed all the AI models: solid volume fraction (ϕ), temperature (T), mean diameter of nanoparticle (D_p), SHC of base fluid (C_P^{Base}), SHC of nanoparticle (C_P^{p}), and density of nanoparticleρ_p.

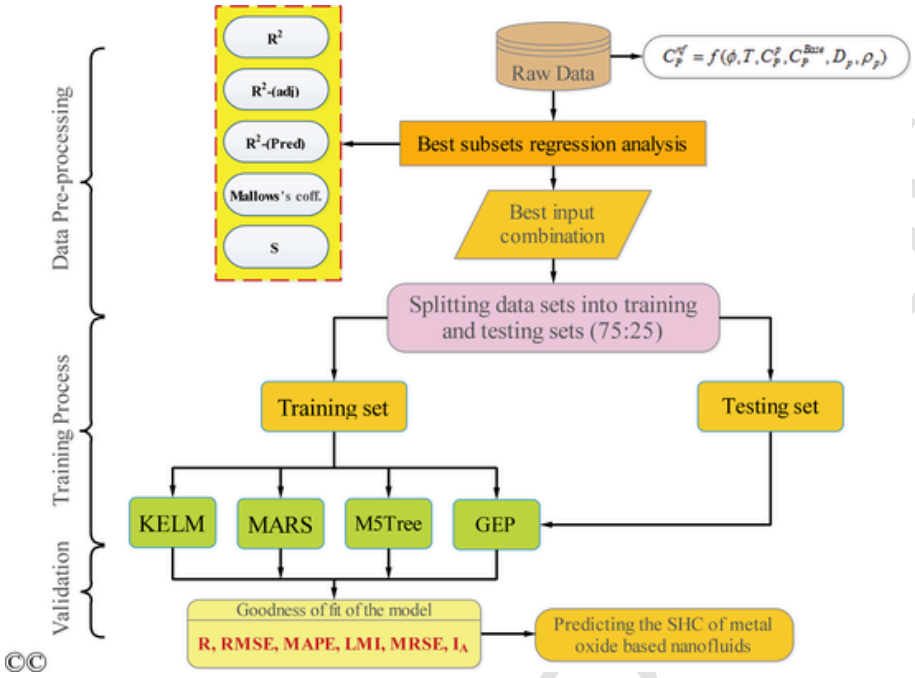

Fig. 6. Road map of predicting process SHC of metal oxide-based nanofluids.

ARESLab, as an open-source code in MATLAB, has been applied to implement the MARS model in the present investigation. In the MARS model's first development, various piecewise linear BFs and order of interactions were examined in a trial and error process. The optimum values of BFs and interactions order were obtained 25 and second-order, respectively, and 3 BFs were pruned in the backward elimination stage. Eventually, the minimum value of the GCV parameter for the optimum MARS model with 22 piecewise linear BFs was obtained by 0.0065. The corresponding coefficients of BFs with the intercept term are listed in Table 6.

Table 6
Basis functions and related coefficients were obtained from the MARS model to predict SHC of metal oxide-based nanofluids.

Basic function	Equation	Coefficientβ_i
intercept	-	2.8118
BF_1	$BF1 = max(0, C_P{}^{Base} - 3.0464)$	0.62284
BF_2	$BF_2 = max(0, \rho_p - 3.6)$	−0.087402
BF_3	$BF_3 = max(0, 3.6 - \rho_p)$	−11.073
BF_4	$BF_4 = BF_1 \times max(0, \phi - 0.5)$	−0.059479
BF_5	$BF_5 = BF_2 \times max(0, C_P{}^{Base} - 3.0925)$	0.86679
BF_6	$BF_6 = BF_2 \times max(0, 3.0925 - C_P{}^{Base})$	0.10473
BF_7	$BF_7 = max(0, D_p - 76)$	0.38605
BF_8	$BF_8 = max(0, 76 - D_p)$	0.0018423
BF_9	$BF_9 = BF_8 \times max(0, \rho_p - 3.6)$	0.0021082
BF_{10}	$BF_{10} = BF_8 \times max(0, 3.6 - \rho_p)$	0.21048
BF_{11}	$BF_{11} = BF_8 \times max(0, C_P{}^{Base} - 4.0889)$	0.053541
BF_{12}	$BF_{12} = BF_8 \times max(0, 4.0889 - C_P{}^{Base})$	−0.008606
BF_{13}	$BF_{13} = BF_2 \times max(0, \phi - 0.4)$	−0.016226
BF_{14}	$BF_{14} = BF_2 \times max(0, 0.4 - \phi)$	1.8847
BF_{15}	$BF_{15} = max(0, T - 329.63)$	−0.0025706
BF_{16}	$BF_{16} = max(0, 329.63 - T)$	−0.0030795
BF_{17}	$BF_{17} = BF_1 \times max(0, \rho_p - 3.9)$	−0.86457
FB_{18}	$BF_{18} = BF_1 \times max(0, 3.9 - \rho_p)$	1.2392
BF_{19}	$BF_{19} = BF_3 \times max(0, T - 319.37)$	−0.01788
BF_{20}	$BF_{20} = BF_3 \times max(0, 319.37 - T)$	−0.0033437
BF_{21}	$BF_{21} = max(0, \phi - 0.5)$	−0.028314
BF_{22}	$BF_{22} = max(0, 0.5 - \phi)$	0.40512

Developing a GEP model based on the GeneXpro Tools has been employed to predict and obtain the predictive correlation based on the simple mathematical operators (i.e., +, -, ×, /, and pow) for SHC of metal oxide-based nanofluids. The setting parameters for developing the GEP model are tabulated in Table 7. Fig. 7 demonstrates the expression tree of the GEP model, which can be used for the estimation of SHC of metal oxide-based nanofluids with (R = 0.9570). The correlation derived from the tree model of GEP is reported in Table 8, which researchers can easily use due to using simple mathematical operators.

To provide the KELM, two crucial hyperparameters, namely, the regularization coefficient (C) and width of kernel function (σ) were optimized by a trial and error procedure. The optimal values of C and σ were obtained from 700000 and 40, respectively. As mentioned before, the KELM network's topology is included 3 layers and six input neurons (equal to input variables).

7. Discussion and result

In the current research, the performance of understudy AI techniques has been assessed using strong statistical measures. Additionally, the statistical results of AI techniques for the training, testing, and all dataset have been given in Tables 9, respectively. From Table 9, the

Table 7
Genetic operators for the GEP model.

GEP parameter	Setting of parameter
Number of chromosomes	30
Head size	7
Number of genes	5
Function set	+, −, ×, /, √, power
Fitness function	RMSE
Mutation rate	0.00138
Inversion rate	0.00546
Gene transposition rate	0.00227
One-point and two-point recombination rate	0.00227
Gene recombination rate	0.00227

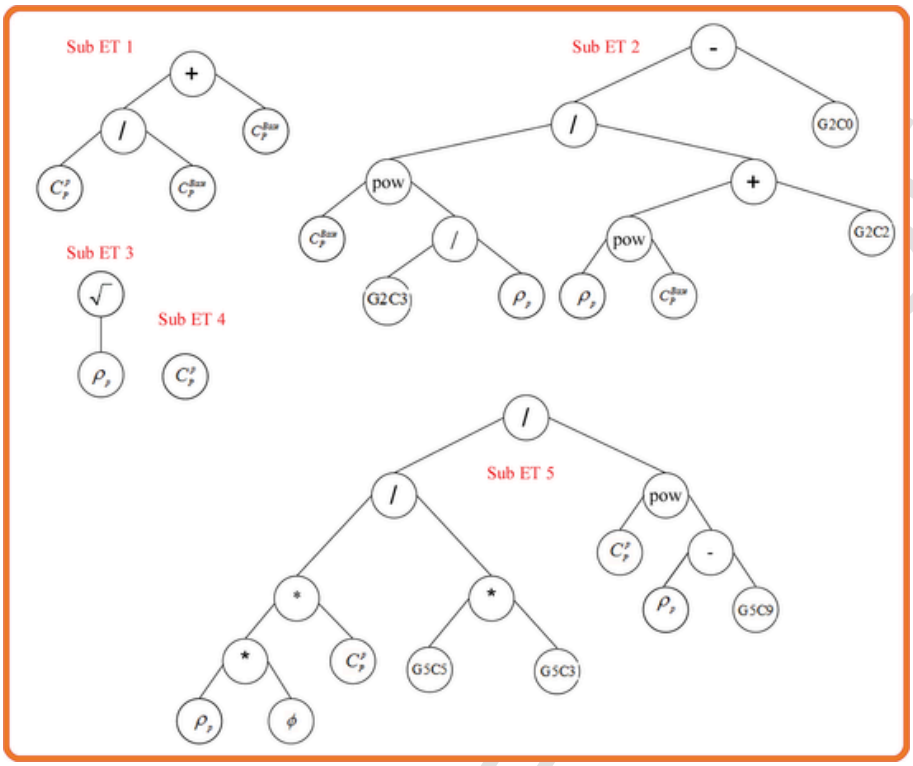

Fig. 7. GEP Expression tree for predicting SHC of metal oxide-based nanofluids using simple mathematical functions (+, -, ×, /, and pow).

Table 8
Equations obtained by the GEP methods to estimate the SHC of metal oxide-based nanofluids.

Model	Formula
GEP:	$C_p^{nf} = \left[C_P^p/C_P^{Base} + C_P^{Base}\right] + \left[\left[C_P^{Base^{(G2C3/\rho_p)}}/\left(\rho_p{}^{C_P^{Base}} + G2C2\right)\right] - G2C0\right] + \sqrt{\rho_p} + C_P^p + \left[\rho_p \phi C_P^p/(G5C5 \times G5C3)\right]/C_P^{p^{(\rho_p - G5C9)}}$; (R = 0.9570) G2C0 = 3.33718810724893; G2C2 = 3.89385662404248; G2C3 = 5.9411497461776; G5C5 = -5.21484928333217; G5C3 = 8.29553994292786; G5C9 = 5.18569750053407;

Table 9
The statistical evaluation of all predictive models for training, testing, and all data sets.

	Metrics	MARS	KELM	M5Tree	GEP
Train	R	0.9935	0.9997	0.9930	0.9593
	RMSE	0.0254	0.0050	0.0273	0.0632
	MAPE	1.9368	0.4149	1.7145	5.3555
	LMI	0.9106	0.9813	0.9192	0.7558
	MSRE	0.0014	0.00004	0.0015	0.0062
	I_A	0.9967	0.9999	0.9961	0.9783
Test	R	0.9892	0.9994	0.9867	0.9500
	RMSE	0.0330	0.0080	0.0370	0.0703
	MAPE	2.3298	0.6152	2.1537	5.9887
	LMI	0.8933	0.9729	0.9029	0.7271
	MSRE	0.0023	0.0001	0.0028	0.0082
	I_A	0.9945	0.9997	0.9928	0.9732
All	R	0.9930	0.9997	0.9921	0.9570
	RMSE	0.0264	0.0059	0.0288	0.0650
	MAPE	1.9826	0.4644	1.7666	5.5134
	LMI	0.9074	0.9793	0.9163	0.7489
	MSRE	0.0012	0.0001	0.0013	0.0067
	I_A	0.9965	0.9998	0.9957	0.9771

results of KELM model indicated the highest correlation (R = 0.9997 and I_A = 0.9998 and LMI = 0.9793) and the least error (RMSE = 0.0059 J/K.g, MAPE = 0.4644%, and MSRE = 0.0001) than MARS (R = 0.9930, RMSE = 0.0264 J/K.g, MAPE = 1.9826% and I_A = 0.9965), M5Tree (R = 0.9921, RMSE = 0.0288 J/K.g, MAPE = 1.7666% and I_A = 0.9957) and GEP (R = 0.9570, RMSE = 0.0650 J/K.g, MAPE = 5.5134% and I_A = 0.9771) models. Furthermore, in the testing phase, the KELM technique with R of 0.997, RMSE of 0.0153 (J/K.g) was significantly determined as the superior predictors for estimating the SHC of nanofluid over standalone AI models. Additionally, the testing phase results indicate that the MARS (R = 0.9892, RMSE = 0.0330 J/K.g, and MAPE = 2.3298) and M5Tree (R = 0.9867, RMSE = 0.0370 J/K.g, and MAPE = 2.1537) models have almost similar efficiency. Fig. 8 shows the spider plots of all statistical performances corresponding to the four developed AI-based models in testing and training datasets. Fig. 9 depicts the graphical assessment of four AI techniques for both training and testing stages. The left column demonstrates the scatter plots, and the right column describes the distribution of predicted datasets compared to experimental values. The C_p^{nf}values given by the KELM model by permissible level of accuracy show the well-matching with laboratory observations those obtained MARS, M5Tree, and GEP techniques. It should be said that MARS, M5, and GEP had the most efficient predictions in the ranges$C_p^{nf} \geq 3$ $C_p^{nf} \geq 3.5$, and $3 \leq C_p^{nf} \leq 4$, respectively.

Error analysis was comprehensively conducted to efficiently assess the precision level of developed techniques by Relative Deviation (RD) ($RD = 100 \times C_p^{nf}/(C_p^{nf} - C_p^{nf})$) and Cumulative Frequency of Absolute Relative Error (CFAE). Fig. 10 demonstrated the distribution associated with the relative deviation for all predictive models in the form of the violin (A) and histogram plot (B) for both training and testing stages. From Fig. 10, the relative deviation probability density of the KELM technique illustrates a high level of compression in the training and testing phase than those observed by MARS, M5Tree, and GEP. Owning to the least range of deviation, evaluation of the RD range in-

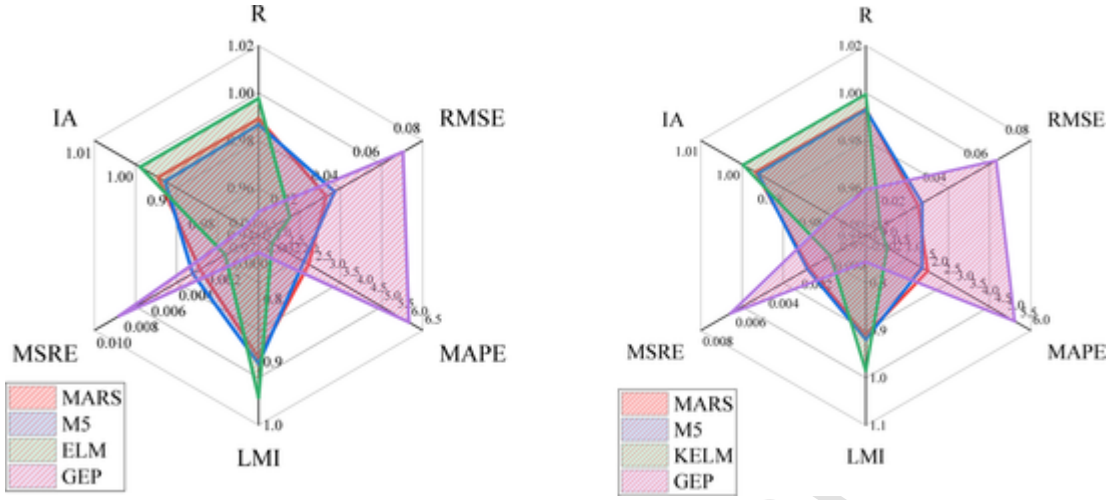

Fig. 8. The spider plot of performance metrics for developed predictive models in training (Left) and testing (Right) phases.

dicated KELM technique ($-4.2\ \% \le RD \le 8.0\%$) had superior performance to the MARS ($-24.8\ \% \le RD \le 15.3\%$), M5Tree ($-30.0\ \% \le RD \le 29.50\%$), and GEP ($-75\ \% \le RD \le 16.6\%$) techniques. Deeply measurement of the relative deviation implies that the underestimation in MARS and GEP model is dominated by the overestimation, whereas in EKELM, this trend is reversed. Besides, MARS and M5Tree techniques have been distributed with less compression than the GEP, which has a higher deviation range between all predictive models.

Moreover, another efficient error analysis has been carried out on the validation of the AI models in predicting SHC of metal oxide-based nanofluids by measuring the variation of percentage of cumulative frequency of absolute relative error (CFAE). As seen in Fig. 11 (Left), over 90% of the estimated SHC (C_p^{nf}) given by the KELM model resulted in Absolute Relative Error (ARE) of lower than 1 %. In contrast, MARS and M5Tree, and GEP models obtained 4.53%, 3.42%, and 12.0%, respectively. Owning to similar performance of MARS and M5Tree techniques, the values of ARE between 0 and 6 percentages have been magnified in Fig. 11 (Right) So that a more comprehensive judgment can be made about their merits. According to Fig. 11 (Right), the MARS approach in the range of 0 to 65% (up to ARE = 6%) of all predicted values brings about more precise results. In contrast, over 65% of the data points, the M5Tree has slightly better predictive performance in estimating SHC. Regarding the results of error analysis, it was inferred that the M5Tree resulted in comparatively better performance (MAPE = 1.7666%) in comparison with the MARS technique (MAPE = 1.9826%), despite having more less correlation for all datasets (R = 0.9921) and higher RMSE (0.0288 J/K.g), stood at the second rank with a highly acceptable precision level in the prediction of SHC.

In the nest stage, a physical trend of SHC for four nanofluids was examined for finding the capabilities of the leading AI models. Then results of consistency between experimental observations and AI models were compared to models 1 and 2. Fig. 12 depicted the variation of SHC three understudy metal oxide-based nanofluid including SiO_2 by $D_p = 22nm$ in a mixture of EG, GC, and GC-EG [121] versus the volume fraction (%) obtained from four AI-based models, experimental data points. Model 1 (Pak and Cho) [88] and Model 2 (Xuan and Roetzel's) [122] As seen in Fig. 12, the results indicated that SHC values predicted by the proposed KELM models results were in good agreement with the measured values and superior to the models 1 and 2.

According to Fig. 13, the physical trend of SHC associated with nanofluids, composed of ZnO in a mixture of W-EG (40:60) by $\phi = 7\ \%\ and\ D_p = 77nm$ [86], against temperature (K) between the range of 310 to 365 (K) were conceptually depicted by using four understudies AI techniques and the models 1 and 2 [88,122]. From Fig. 13, it can be said that the KELM model was prosperous in obtaining the physical meaning of experimental data sets. The M5Tree model for rang of ($315 \le T < 340\ K$) has better agreement with experimental values than MARS, whereas the MARS model outperforms M5Tree for rang of ($340 \le T \le 365\ K$).

In the last validation case, the variation of Al_2O_3/R134a oil [90] at $\phi = 5\%$ versus the temperature (K) in the AI models' performance measurement is illustrated in Fig. 14. The KELM technique can obtain optimally the expected physical trend of the pertaining experimental data points followed by MARS, M5Tree, and GEP techniques. Eventually, it can be declared that the KELM model is superior to the other machine learning-based models for accurately estimating SHC of metal oxide-based nanofluids.

8. Robustness evaluation of models

According to the Vajjha and Das [123] investigations, the existing correlation cannot accurately estimate nanofluids' SHC. Thus, they presented an individual correlation based on ϕ, T, $C_P{}^P$ and $C_P{}^{Base}$ for three metal oxides, namely, Al_2O_3, ZnO, and SiO_2 mixture in water and W-EG (40:60), which had good agreement with the observed value of SHC with a maximum deviation of 5%, 4.4%, and 3.1%. the Vajjha and Das [123] correlation is expressed as follows:

$$\frac{C_P^{nf}}{C_P^{Base}} = \frac{A \times \left(\frac{T}{T_0}\right) + B \times \left(\frac{C_P^P}{C_P^{Base}}\right)}{(C + \phi)} \tag{31}$$

T denotes the reference temperature (T0 = 273K), A, B, and C are the curve-fit coefficient. The curve-fit coefficients for each metal oxide are listed in Table 10.

In this section, the robustness of developed AI models for Al_2O_3, ZnO, and SiO_2 based nanofluids in the validity ranges of the modified Vajjha and Das [123] correlations are examined.

Regarding Table 11, the result indicated that for ZnO based nanofluids, the KELM terms of (R = 0.9981 and RMSE = 0.0052) has the best performance, followed by MARS (R = 0.9767 and RMSE = 0.018), M5Tree (R = 0.9555 and RMSE = 0.0322), Vajjha & Das [123] (R = 0.7850 and RMSE = 0.0830), and GEP (R = 0.7562 and RMSE = 0.0656). For the Al_2O_3 nanofluids, all developed soft computing-based models outperformed the Vajjha & Das [123] correlation. The metric performance in Table 11 reported promising simulation results for KELM with around 30% precision improvement compared

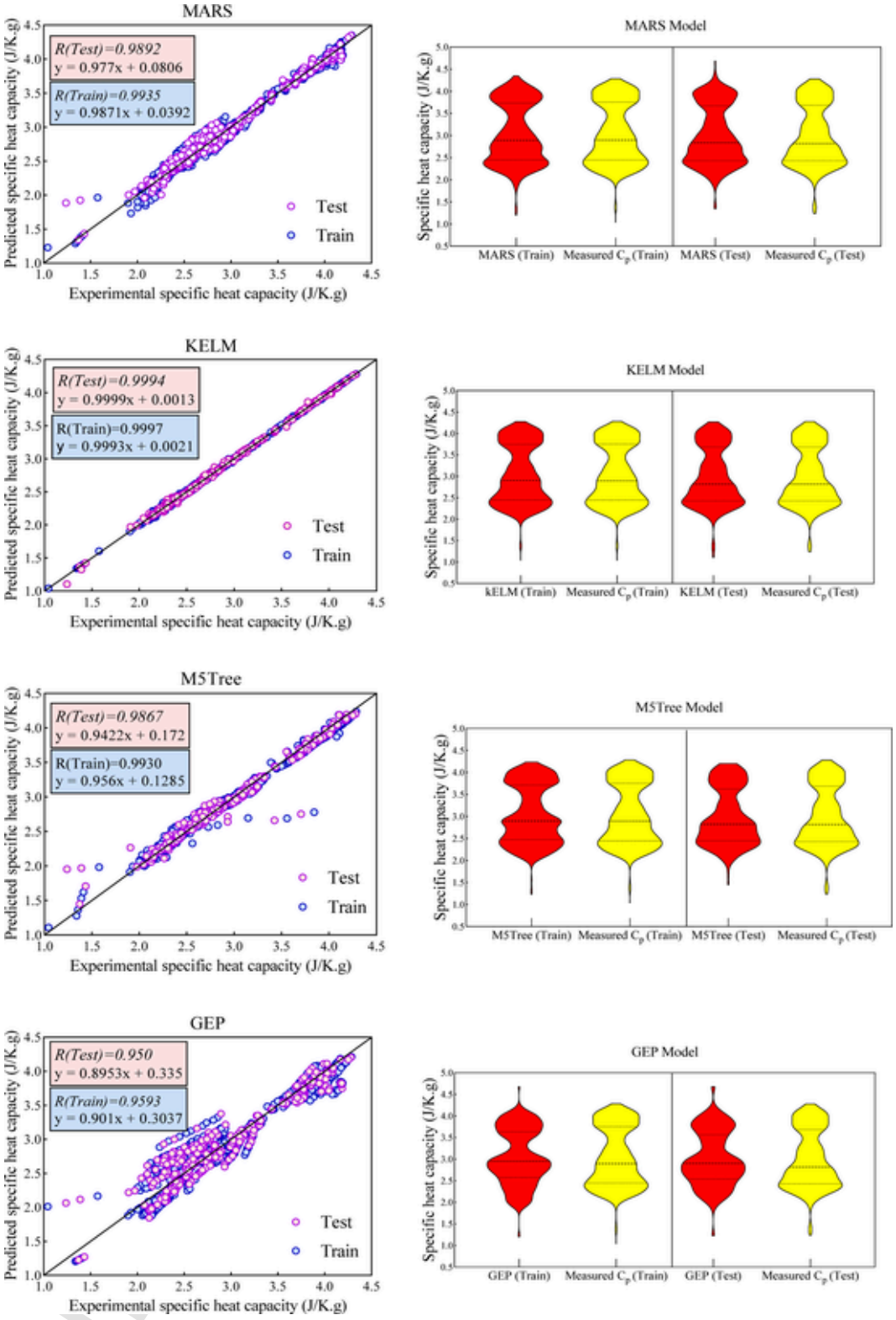

Fig. 9. The scatter plot of four AI models (Left) and the distribution of predicted value compared with an experimental dataset for both testing and training phases.

with Vajjha & Das [123] correlation. Besides, for SiO_2 based nanofluids in the validity ranges of ($315 \leq T < 363$, $\phi \leq 7\%$), KELM (R = 0.9987) and MARS (R = 0.9754) had a successful performance in the estimation of SHC. Simultaneously, the GEP and Vajjha & Das [123] correlation results showed a very similar accuracy. Fig. 15 illustrated the degree

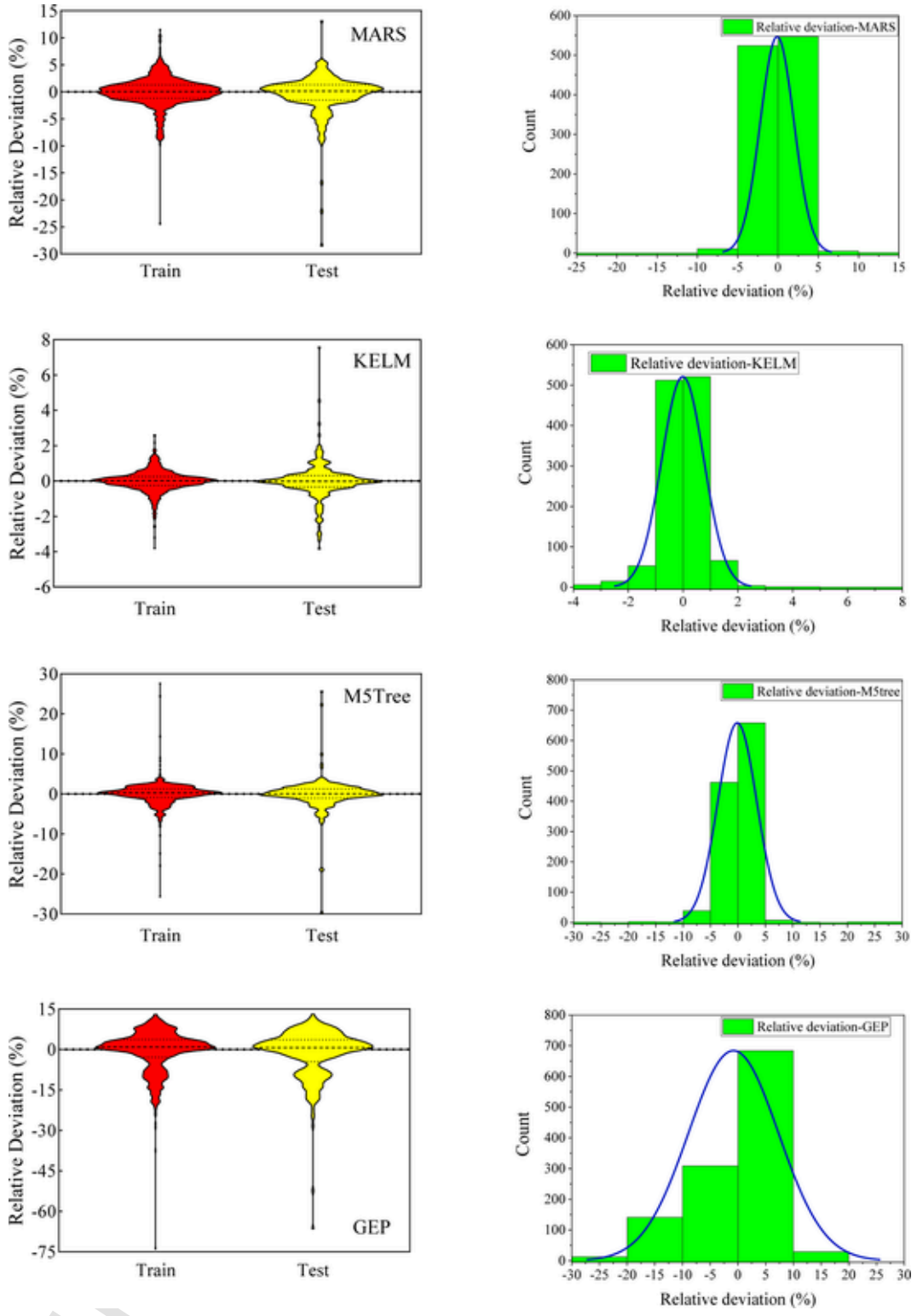

Fig. 10. The probability density of relative deviation (Left) and frequency distribution histogram of relative deviation frequency for all AI models.

of conformity of modeling and observational SHC values obtained by the KELM, MARS, M5Tree, GEP, and Vajjha & Das [123].

9. Sensitivity analysis

One of the essential parts of under predictive study models is sensitivity analysis, which can help to properly select the predictor parameters (i.e., ϕ, T, C_P^p, C_P^{Base}, D_p, ρ_p) in a miserable range in modeling and consequently enhance the accuracy of the AI-based model. Based on the Pearson correlation between the independent and the target variable in the data preprocessing stage, SHC of base fluid (C_P^{Base}) with the most value of correlation coefficient ($r_p = 0.79$) was taken into account to be the most significant predictor. According to the non-linear trend among independent and dependent variables, the relative significance

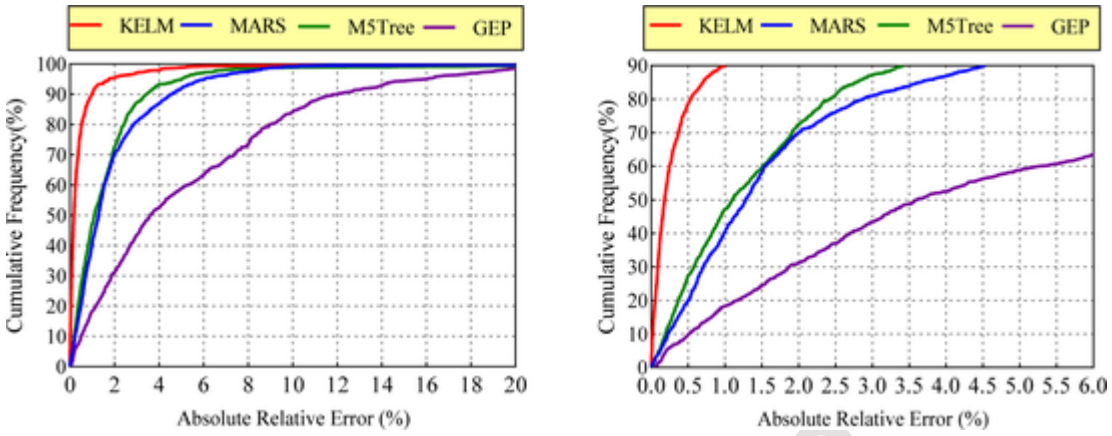

Fig. 11. The cumulative frequency against absolute relative error (deviation) for four soft computing models in minimized scale (Left) and originally scale (Right).

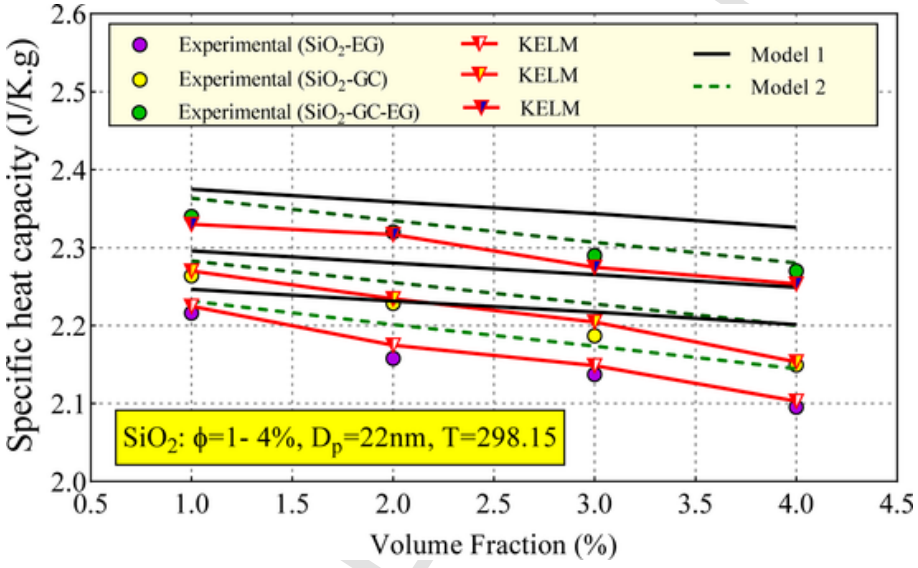

Fig. 12. Comparing the predicted SHC using the KELM model, Model 1, Model 2, and experimental datasets for thee nanofluids consist of SiO_2 by ϕ = 1, 2, 3, 4% in an EG, GC, and GC-EG [121].

of the predictors is precisely evaluated by subsequent elimination of a given input and preserving the other inputs for feeding the AI technique [58,124,125]. In this approach, the KELM technique, as the most efficient AI model, has been selected to survey the response of SHC based upon the degree of influence of each input in terms of the statistical measures.

As seen in Table 12 and Fig. 16, it was found that $C_P^{Base}$with the lowest correlation coefficient (R = 0.7043) and having the most error metrics (RMSE = 0.1589 J/K.g and MAPE = 11.5986 %) is introduced as the most sensitive input variable in the evaluation of the SHC of nanofluids. Additionally, the volume fraction (R = 0.9528 and RMSE = 0.0684 J/K.g) and SHC of nanoparticles (R = 0.9865 and RMSE = 0.0372 J/K.g) stood at the 2nd and 3rd ranks. In Fig. 16, it was conveniently found that the temperature (R = 0.9977 and RMSE = 0.0153 J/K.g) is identified as the least influential input variable in predicting the SHC of nanofluids.

10. Qualitative response assessment of SHC upon influence features

In this section, a brief qualitative response analysis is adopted to evaluate the SHC variations against effective features. For this purpose, the 2D counters of SHC of metal oxide-based nanofluids were plotted in terms of C_P^P and ϕ as the effective features, for Water, EG, and a mixture of water and EG, as the most common base fluids, in Fig 17. The SHC response analysis from the contours illustrates that in a generalized hypothesis, the decreasing the SHC of C_P^{Base}yield the reduction of SHC of nanofluids. Table 13 listed the thermo-physical properties of metal oxide nanoparticles and base fluids used in model development. Carefully assessing the contours inferred the below results:

- Measuring the metal oxide dispersed in water (DW/W) nanofluids (Fig. 17-A) indicated that for $\phi \geq 4$, MgO, TiO_2, and ZnO are the most influential metal oxide in significantly decreasing the SHC of water, respectively and, as MgO can reduce the over 25% of SHC of water. The reduction performance of SiO_2 was found in the intermediated level.
- Fig. 17-B demonstrated that the Al_2O_3 and CuO are the most influential metal oxide, which can adequately reduce the SHC of the base fluid in understudy ethylene glycol-based nanofluids up to 50%, respectively. The range of $3 \leq \phi \leq 6$ in the qualitative judgment is found as the optimum values of nanoparticle volume fraction.
  Fig. 17C inferred that for the metal oxide-based nanofluids dispersed in a mixture of water and ethylene glycol, the CuO, ZnO, MgO in range of $\phi \geq 5$ having promising performance in reducing the capacity of the base fluid compared to other metal oxides, respectively.

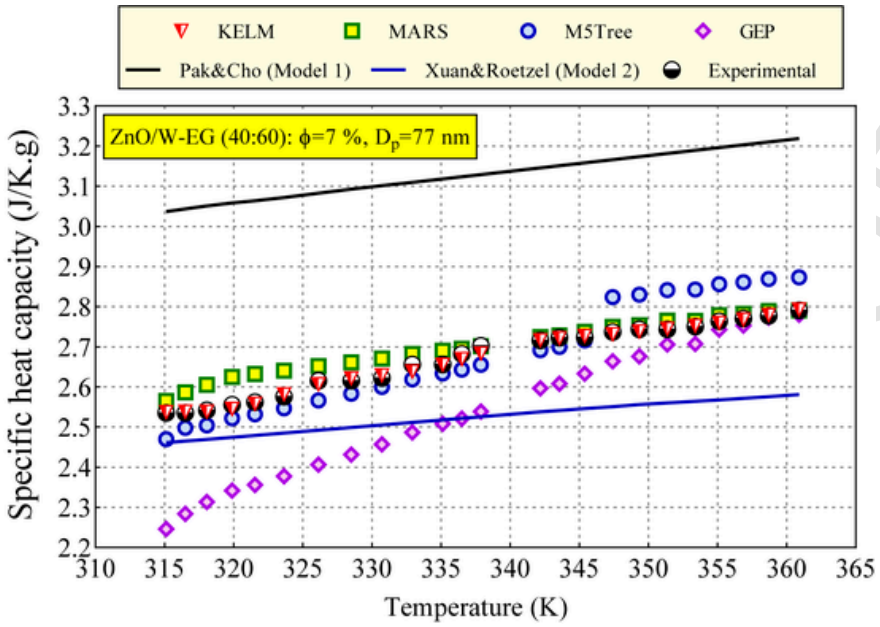

Fig. 13. Comparing the predicted SHC using four AI models, Pak% Cho (Model 1), Xuan&Roetzel (Model 2), and experimental datasets for nanofluids consist of ZnO in a mixture of W-EG (40:60) [86].

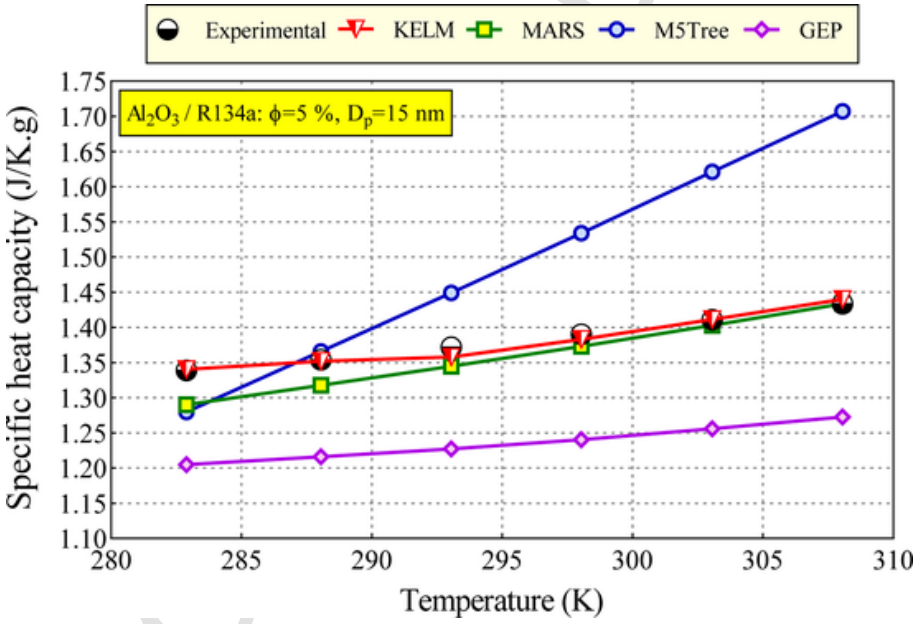

Fig. 14. Comparing the predicted SHC using developed AI-based model and experimental datasets for metal oxide-based nanofluids consist Al_2O_3 by ϕ = 5% in R134a oil as base fluid [90].

Table 10
Curve-fit coefficients for SHC of three metal oxide-based nanofluids [123].

Nanofluid	A	B	C	Validity Ranges
Al_2O_3	0.24327	0.5179	0.4250	$315 \le T < 363$, $\phi \le 10\%$
SiO_2	0.48294	1.1937	0.8021	$315 \le T < 363$, $\phi \le 7\%$
ZnO	0.12569	0.9855	0.299	$315 \le T < 363$, $\phi \le 10\%$

11. Conclusion and remarks

The current research aimed to provide a robust ML model, namely, the KELM model, to estimate SHC for a broad range of metal oxide-based nanofluids. Moreover, three AI models (i.e., MARS, m5Tree, and GEP) have been applied to compare the results. To perform the training and testing phases, 1180 experimental datasets have been accumulated from authenticated literature. The best input variables explored are based on the best subset analysis, which contains six predictors comprised of ϕ, T, C_P^p, C_P^{Base}, D_p *and* ρ_p.

Table 11
Statistical evaluation for SHC of three metal oxide-based nanofluids using AI-based models and Vajjha & Das [123].

	Metrics	Vajjha&Das	KELM	MARS	M5Tree	GEP
ZnO	R	0.7850	0.9981	0.9767	0.9555	0.7562
	RMSE	0.0830	0.0052	0.0180	0.0322	0.0656
	MAPE%	6.8283	0.3706	1.3835	2.4383	5.6687
	E	0.0593	0.9475	0.7995	0.6458	0.1730
	MSRE	0.0080	0.0000	0.0003	0.0010	0.0041
	IA	0.7508	0.9990	0.9879	0.9501	0.8012
	Rank	4	1	2	3	5
Al_2O_3	R	0.7607	0.9978	0.9260	0.9770	0.8777
	RMSE	0.0712	0.0050	0.0287	0.0163	0.0397
	MAPE%	5.9119	0.3817	2.0775	1.0960	3.1320
	E	0.1401	0.9397	0.6455	0.8137	0.2510
	MSRE	0.0047	0.0000	0.0008	0.0003	0.0016
	IA	0.8028	0.9989	0.9609	0.9873	0.8987
	Rank	5	1	2	3	4
SiO_2	R	0.8013	0.9987	0.9754	0.8857	0.8010
	RMSE	0.0520	0.0027	0.0147	0.0403	0.0445
	MAPE%	2.8406	0.2118	0.9944	2.6235	3.3032
	E	0.4238	0.9524	0.8009	0.5499	0.4184
	MSRE	0.0021	0.0000	0.0002	0.0028	0.0018
	IA	0.8181	0.9994	0.9836	0.8997	0.8688
	Rank	5	1	2	3	4

- Results of quantitative comparisons indicated that the KELM model with R of 0.9994, RMSE of 0.0080 J/K.g, and MAPE = 0.6152% resulted in a highly satisfying accuracy level in the assessment of SHC for understudy metal oxide-based nanofluids when compared to MARS ($I_A = 0.9892$, RMSE = 0.0330 J/K.g, and MAPE = 2.3298%), M5Tree ($I_A = 0.9867$, RMSE = 0.0370 J/K.g and MAPE = 2.1537%) and GEP ($I_A = 0.950$, RMSE = 0.0703 J/K.g and MAPE = 5.9887%) in the testing phase.
- Error analysis of the AI results demonstrated that the MARS and M5Tree model's physical variations of the SHC parameter have almost similar predictive performance. In addition to this, the physical trend assessment of SHC of ZnO in a mixture of W-EG (40:60) indicated that the MARS model predicted values in high temperatures were in good agreement with the experimental SHC than those obtained by M5Tree and vice versa.
- The robustness of the developed soft computing models was measured by comparing with the Vajjha & Das correlation for Al_2O_3, ZnO, and SiO_2 based nanofluids, which AI models were more efficient and accurate than Vajjha & Das correlation except for ZnO based nanofluids.
- A qualitative response assessment of SHC of nanofluids was carried out for three common base fluids, namely, Water, ethylene glycol, and a mixture of water and ethylene glycol, which of all the studied oxides, CuO, ZnO, and MgO had a relatively more effective performance in reducing the SHC of the base fluids.
- Results of the sensitivity analysis indicated that omitting the SHC of base fluid (C_P^{Base}) and temperature (T) in the KELM model yield the worst (R = of 0.7043 and RMSE of 0.1589 J/K.g) and best results, respectively. Thus, it can significantly infer that C_P^{Base} and is identified as the most influential predictor in assessing SHC of nanofluids among all the independent predictive variables. In contrast, the temperature (T) as the least important feature can be ignored in SHC of metal oxide-based nanofluids modeling.

Credit author statement

M. Jamei was responsible for Conceptualization, Methodology, Writing- Original draft preparation. I. Ahamdianfar, I. A. olumegbon, M. Karbasi, Z. Said, M. Sharifpur, and J. P, Meyer were responsible for formal analysis, validation, and data curation. A. Asadi was responsible reviewing and editing the manuscript and supervising the project.

Declaration of Competing Interest

The authors declare that they have no known competing financial interests or personal relationships that could have appeared to influence the work reported in this paper.

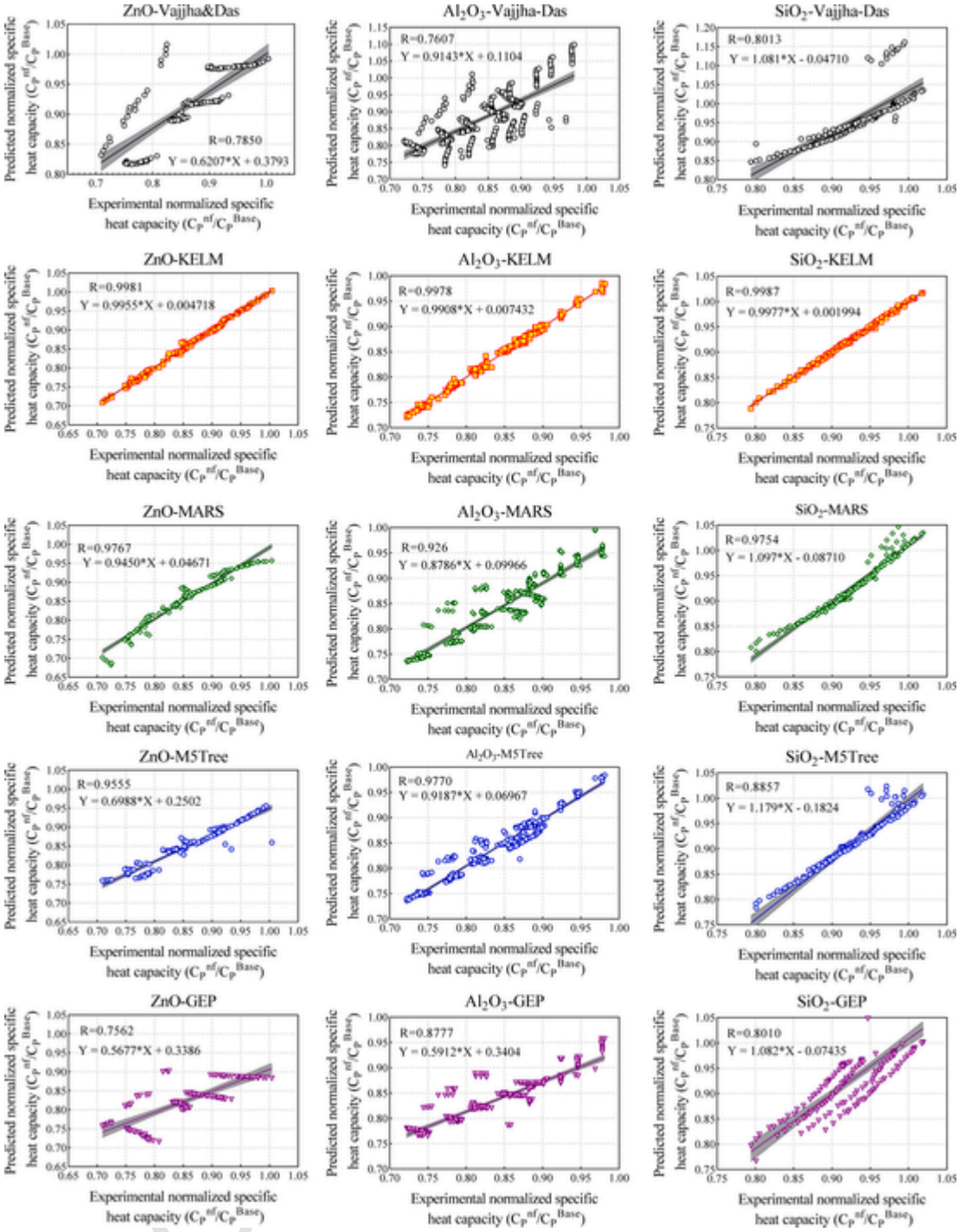

Fig. 15. The performance comparison between Vajjha & Das [123] and developed AI models in predicting SHC of AL_2O_3, ZnO, and SiO_2 based nanofluids.

Table 12
The sensitivity analysis via the KELM model.

	All-φ	All-T	All-$C_P{}^{p}$	All-$C_P{}^{Base}$	All-D_p	All-ρ_p	All
R	0.9528	0.9977	0.9865	0.7043	0.9873	0.9972	0.9994
RMSE	0.0684	0.0153	0.0372	0.1589	0.0358	0.0173	0.0080
MAPE	5.7832	0.9895	2.0380	11.5986	2.4084	1.1442	0.6152
I_A	0.9752	0.9988	0.9931	0.8155	0.9934	0.9985	0.9997
Rank	2	6	3	1	4	5	–

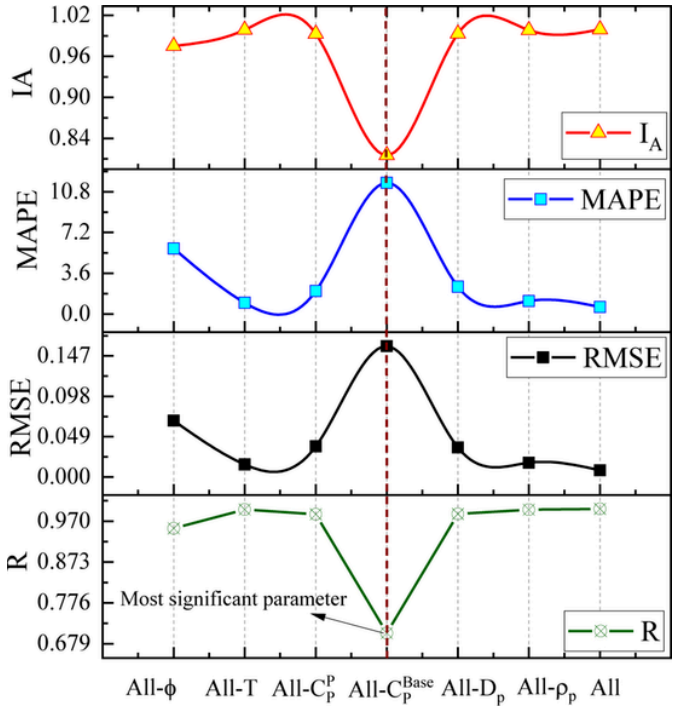

Fig. 16. The statistical parameters for all sensitivity analysis situations which obtained by the KELM model.

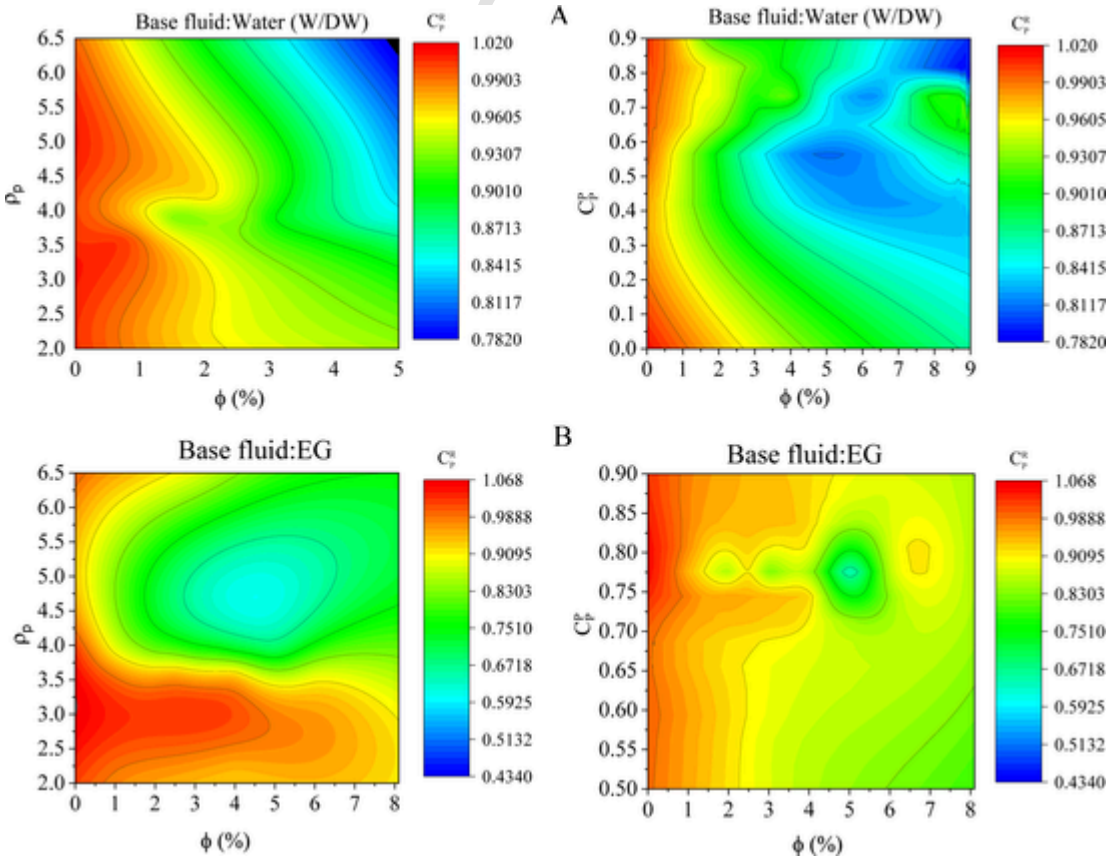

Fig. 17. Assessment of the qualitative SHC response upon influence features for metal oxide nanofluid in different base fluids.

Table 13
Thermo-physical properties of all existing metal oxide nanoparticles and base fluids in the database [126–128].

Metal oxide	AL_2O_3	CuO	SiO_2	ZnO	TiO_2	MgO
Cp (J/K.g)	0.765	0.53	0.745	0.514	0.683	0.877
ρ_p(gr/cm ^{3})	3.60	6.50	2.20	5.60	4.20	3.58
Base fluids	Water	EG	W(DW)/EG	R134a	W-PG	EG-CG/CG
Rang of Cp (J/K.g)	4.05-4.2	2.4-2.61	3.08-3.72	1.37-1.47	3.05-3.5	2.3-2.48

References

[1] M.A. Ariana, B. Vaferi, G. Karimi, Prediction of thermal conductivity of alumina water-based nanofluids by artificial neural networks, Powder Technol. 278 (2015) 1–10, doi:10.1016/J.POWTEC.2015.03.005.

[2] S.S. Soleimani, S. Jahandari, S. Aberoumand, A. Rahmani, A. Shokrgozar, Cu/Oil nanofluids flow over a semi-infinite plate accounting an experimental model, Heat Transf. Res. (2020), doi:10.1002/htj.21664.

[3] S. Aberoumand, A. Jafarimoghaddam, Experimental study on synthesis, stability, thermal conductivity and viscosity of Cu–engine oil nanofluid, J. Taiwan Inst. Chem. Eng. 71 (2017) 315–322, doi:10.1016/J.JTICE.2016.12.035.

[4] A. Asadi, A.N. Bakhtiyari, I.M. Alarifi, Predictability evaluation of support vector regression methods for thermophysical properties, heat transfer performance, and pumping power estimation of MWCNT/ZnO–engine oil hybrid nanofluid, Eng. Comput. (2020) 1–11, doi:10.1007/s00366-020-01038-3.

[5] A.A. Hachicha, Z. Said, S.M.A. Rahman, E. Al-Sarairah, On the thermal and thermodynamic analysis of parabolic trough collector technology using industrial-grade MWCNT based nanofluid, Renew. Energy. 161 (2020) 1303–1317.

[6] M. Ghodbane, Z. Said, A.A. Hachicha, B. Boumeddane, Performance assessment of linear Fresnel solar reflector using MWCNTs/DW nanofluids, Renew. Energy. 151 (2020) 43–56.

[7] Z. Lyu, F. Pourfattah, A.A.A. Arani, A. Asadi, L.K. Foong, On the thermal performance of a fractal microchannel subjected to water and kerosene carbon nanotube nanofluid, Sci. Rep. 10 (2020) 7243, doi:10.1038/s41598-020-64142-w.

[8] Z. Lyu, A. Asadi, I.M. Alarifi, V. Ali, L.K. Foong, Thermal and fluid dynamics performance of MWCNT-water nanofluid based on thermophysical properties: an experimental and theoretical study, Sci. Rep. 10 (2020) 5185, doi:10.1038/s41598-020-62143-3.

[9] M. Mahdavi, M. Sharifpur, J.P. Meyer, Exploration of nanofluid pool boiling and deposition on a horizontal cylinder in Eulerian and Lagrangian frames, Int. J. Heat Mass Transf. 125 (2018) 959–971.

[10] R. Ranjbarzadeh, A. Moradikazerouni, R. Bakhtiari, A. Asadi, M. Afrand, An experimental study on stability and thermal conductivity of water/silica nanofluid: Eco-friendly production of nanoparticles, J. Clean. Prod. 206 (2019) 1089–1100.

[11] A. Asadi, S. Aberoumand, A. Moradikazerouni, F. Pourfattah, G. Żyła, P. Estellé, O. Mahian, S. Wongwises, H.M. Nguyen, A. Arabkoohsar, Recent advances in preparation methods and thermophysical properties of oil-based nanofluids: A state-of-the-art review, Powder Technol. 352 (2019) 209–226, doi:10.1016/j.powtec.2019.04.054.

[12] A. Asadi, F. Pourfattah, I. Miklós Szilágyi, M. Afrand, G. Żyła, H. Seon Ahn, S. Wongwises, H. Minh Nguyen, A. Arabkoohsar, O. Mahian, Effect of sonication characteristics on stability, thermophysical properties, and heat transfer of nanofluids: A comprehensive review, Ultrason. Sonochem. 58 (2019) 104701, doi:10.1016/J.ULTSONCH.2019.104701.

[13] N. Ali, J.A. Teixeira, A. Addali, A review on nanofluids: fabrication, stability, and thermophysical properties, J. Nanomater. 2018 (2018) 1–33, doi:10.1155/2018/6978130.

[14] O. Mahian, L. Kolsi, M. Amani, P. Estellé, G. Ahmadi, C. Kleinstreuer, J.S. Marshall, M. Siavashi, R.A. Taylor, H. Niazmand, O. Mahian, L. Kolsi, M. Amani, P. Estellé, G. Ahmadi, Recent advances in modeling and simulation of nanofluid flows-Part I Fundamentals and theory To cite this version: HAL Id: hal-02051320, Phys. Rep. (2019), doi:10.1016/j.physrep.2018.11.004.

[15] O. Mahian, L. Kolsi, M. Amani, P. Estellé, G. Ahmadi, C. Kleinstreuer, J.S. Marshall, R.A. Taylor, E. Abu-Nada, S. Rashidi, H. Niazmand, S. Wongwises, T. Hayat, A. Kasaeian, I. Pop, Recent advances in modeling and simulation of nanofluid flows—Part II: Applications, Phys. Rep. 791 (2019) 1–59, doi:10.1016/j.physrep.2018.11.003.

[16] R. Saidur, T.C. Meng, Z. Said, M. Hasanuzzaman, A. Kamyar, Evaluation of the effect of nanofluid-based absorbers on direct solar collector, Int. J. Heat Mass Transf. 55 (2012) 5899–5907.

[17] A. Hajatzadeh Pordanjani, S. Aghakhani, M. Afrand, B. Mahmoudi, O. Mahian, S. Wongwises, An updated review on application of nanofluids in heat exchangers for saving energy, Energy Convers. Manag. 198 (2019) 111886, doi:10.1016/j.enconman.2019.111886.

[18] M.S. Sadeghi, N. Anadalibkhah, R. Ghasemiasl, T. Armaghani, A.S. Dogonchi, A.J. Chamkha, H. Ali, A. Asadi, On the natural convection of nanofluids in diverse shapes of enclosures: an exhaustive review, J. Therm. Anal. Calorim. (2020) 1–22, doi:10.1007/s10973-020-10222-y.

[19] S. Aberoumand, P. Woodfield, B. Shabani, D.V. Dao, Advances in electrode and electrolyte improvements in vanadium redox flow batteries with a focus on the nanofluidic electrolyte approach, Phys. Rep. (2020), doi:10.1016/j.physrep.2020.08.001.

[20] Z. Said, A.A. Hachicha, S. Aberoumand, B.A.A. Yousef, E.T. Sayed, E. Bellos, Recent advances on nanofluids for low to medium temperature solar collectors: energy, exergy, economic analysis and environmental impact, Prog. Energy Combust. Sci. 84 (2021) 100898, doi:10.1016/j.pecs.2020.100898.

[21] S. Almurtaji, N. Ali, J.A. Teixeira, A. Addali, On the role of nanofluids in thermal-hydraulic performance of heat exchangers—a review, Nanomaterials. 10 (2020) 734, doi:10.3390/nano10040734.

[22] K. Farhana, K. Kadirgama, M.M. Rahman, D. Ramasamy, M.M. Noor, G. Najafi, M. Samykano, A.S.F. Mahamude, Improvement in the performance of solar collectors with nanofluids — a state-of-the-art review, Nano-Structures and Nano-Objects. 18 (2019) 100276, doi:10.1016/j.nanoso.2019.100276.

[23] A. Alshayji, A. Asadi, I.M. Alarifi, On the heat transfer effectiveness and pumping power assessment of a diamond-water nanofluid based on thermophysical properties: An experimental study, Powder Technol. 373 (2020) 397–410, doi:10.1016/j.powtec.2020.06.068.

[24] M. Karami, M.A. Akhavan-Bahabadi, S. Delfani, M. Raisee, Experimental investigation of CuO nanofluid-based direct absorption solar collector for residential applications, Renew. Sustain. Energy Rev. 52 (2015) 793–801, doi:10.1016/j.rser.2015.07.131.

[25] P. Selvakumar, S. Suresh, Convective performance of CuO/water nanofluid in an electronic heat sink, Exp. Therm. Fluid Sci. 40 (2012) 57–63, doi:10.1016/j.expthermflusci.2012.01.033.

[26] M.N. Pantzali, A.G. Kanaris, K.D. Antoniadis, A.A. Mouza, S.V. Paras, Effect of nanofluids on the performance of a miniature plate heat exchanger with modulated surface, Int. J. Heat Fluid Flow. 30 (2009) 691–699, doi:10.1016/j.ijheatfluidflow.2009.02.005.

[27] S.Q. Zhou, R. Ni, Measurement of the specific heat capacity of water-based Al2 O3 nanofluid, Appl. Phys. Lett. 92 (2008), doi:10.1063/1.2890431.

[28] A.K. Starace, J.C. Gomez, J. Wang, S. Pradhan, G.C. Glatzmaier, Nanofluid heat capacities, J. Appl. Phys. 110 (2011) 124323, doi:10.1063/1.3672685.

[29] M. Chandrasekar, S. Suresh, T. Senthilkumar, Mechanisms proposed through experimental investigations on thermophysical properties and forced convective heat transfer characteristics of various nanofluids - A review, Renew. Sustain. Energy Rev. 16 (2012) 3917–3938, doi:10.1016/j.rser.2012.03.013.

[30] H. Nieh, T. Teng, C. Yu, International journal of thermal sciences enhanced heat dissipation of a radiator using oxide nano-coolant, Int. J. Therm. Sci. 77 (2014) 252–261, doi:10.1016/j.ijthermalsci.2013.11.008.

[31] D. Shin, D. Banerjee, Enhancement of specific heat capacity of high-temperature silica-nanofluids synthesized in alkali chloride salt eutectics for solar thermal-energy storage applications, Int. J. Heat Mass Transf. 54 (2011) 1064–1070, doi:10.1016/j.ijheatmasstransfer.2010.11.017.

[32] P.K. Namburu, D.P. Kulkarni, A. Dandekar, D.K. Das, Experimental investigation of viscosity and specific heat of silicon dioxide nanofluids, Micro Nano Lett. 2 (2007) 67–71, doi:10.1049/mnl:20070037.

[33] Q. He, S. Wang, M. Tong, Y. Liu, Experimental study on thermophysical properties of nanofluids as phase-change material (PCM) in low temperature cool storage, Energy Convers. Manag., Pergamon, 2012, pp. 199–205, doi:10.1016/j.enconman.2012.04.010.

[34] L. Lu, Z.H. Liu, H.S. Xiao, Thermal performance of an open thermosyphon using nanofluids for high-temperature evacuated tubular solar collectors. Part 1: Indoor experiment, Sol. Energy. 85 (2011) 379–387, doi:10.1016/j.solener.2010.11.008.

[35] S. K.S, L.V. V, R. K.S, ZnO–propylene glycol–water nanofluids with improved properties for potential applications in renewable energy and thermal management, Colloids Surfaces A Physicochem. Eng. Asp. 506 (2016) 63–73, doi:10.1016/j.colsurfa.2016.06.007.

[36] T. Yousefi, F. Veysi, E. Shojaeizadeh, S. Zinadini, An experimental investigation on the effect of Al2O3-H2O nanofluid on the efficiency of flat-plate solar collectors, Renew. Energy. 39 (2012) 293–298, doi:10.1016/j.renene.2011.08.056.

[37] J.J. Michael, S. Iniyan, Performance of copper oxide/water nanofluid in a flat plate solar water heater under natural and forced circulations, Energy Convers. Manag. 95 (2015) 160–169, doi:10.1016/j.enconman.2015.02.017.

[38] B. Barbés, R. Páramo, E. Blanco, M.J. Pastoriza-Gallego, M.M. Piñeiro, J.L. Legido, C. Casanova, Thermal conductivity and specific heat capacity measurements of Al 2O3 nanofluids, J. Therm. Anal. Calorim. 111 (2013) 1615–1625, doi:10.1007/s10973-012-2534-9.

[39] R. Pa, B. Barbe, E. Blanco, C. Casanova, Thermal conductivity and specific heat capacity measurements of CuO nanofluids, 2014, pp. 1883–1891, doi:10.1007/s10973-013-3518-0.

[40] D.K. Das, Specific heat measurement of three nanofluids and development of new correlations, J. Heat Transf. 131 (2013) 1–7, doi:10.1115/1.3090813.

[41] M.M. Elias, I.M. Mahbubul, R. Saidur, M.R. Sohel, I.M. Shahrul, S.S. Khaleduzzaman, S. Sadeghipour, Experimental investigation on the thermo-physical properties of Al 2 O 3 nanoparticles suspended in car radiator coolant ☆, Int. Commun. Heat Mass Transf. 54 (2014) 48–53, doi:10.1016/j.icheatmasstransfer.2014.03.005.

[42] S.M.S. Murshed, Determination of effective specific heat of nanofluids, 8080, 2011, doi:10.1080/17458080.2010.498838.

[43] S. Zhou, R. Ni, Measurement of the specific heat capacity of water-based Al2O3 nanofluid Measurement of the specific heat capacity of water-based Al 2 O 3 nanofluid, 093123, 2012, pp. 1–4, doi:10.1063/1.2890431.

[44] A.K. Starace, J.C. Gomez, J. Wang, S. Pradhan, G.C. Glatzmaier, A.K. Starace, J.C. Gomez, J. Wang, S. Pradhan, G.C. Glatzmaier, Nanofluid heat capacities Nanofluid heat capacities, 124323, 2011, doi:10.1063/1.3672685.

[45] M.M. Heyhat, F. Kowsary, A.M. Rashidi, M.H. Momenpour, A. Amrollahi, Experimental investigation of laminar convective heat transfer and pressure drop

of water-based Al 2 O 3 nanofluids in fully developed flow regime, Exp. Therm. Fluid Sci. 44 (2013) 483–489, doi:10.1016/j.expthermflusci.2012.08.009.
[46] H. O'Hanley, J. Buongiorno, T. McKrell, L.W. Hu, Measurement and model correlation of specific heat capacity of water-based nanofluids with silica, alumina and copper oxide nanoparticles, ASME 2011 Int, Mech. Eng. Congr. Expo. IMECE 2011 (10) (2011) 1209–1214, doi:10.1115/imece2011-62054.
[47] S. Akilu, A.T. Baheta, K.V. Sharma, M.A. Said, Experimental determination of nanofluid specific heat with SiO2 nanoparticles in different base fluids, AIP Conf. Proc. 2017 (1877), doi:10.1063/1.4999896.
[48] I.H. Alhajri, I.M. Alarifi, A. Asadi, H.M. Nguyen, H. Moayedi, A general model for prediction of BaSO4 and SrSO4 solubility in aqueous electrolyte solutions over a wide range of temperatures and pressures, J. Mol. Liq. (2019), doi:10.1016/j.molliq.2019.112142.
[49] I.A, M.B. Ali Naseri, Mehdi Jamei, Nanofluids thermal conductivity prediction applying a novel hybrid data-driven model validated using monte carlo based sensitivity analysis, Eng. Comput. (2020), doi:10.1007/s00366-020-01163-z.
[50] A.N. Bakhtiyari, Z. Wang, L. Wang, H. Zheng, A review on applications of artificial intelligence in modeling and optimization of laser beam machining, Opt. Laser Technol. 135 (2021) 106721, doi:10.1016/j.optlastec.2020.106721.
[51] I.O. Alade, T.A. Oyehan, I.K. Popoola, S.O. Olatunji, A. Bagudu, Modeling thermal conductivity enhancement of metal and metallic oxide nanofluids using support vector regression, Adv. Powder Technol. 29 (2018) 157–167, doi:10.1016/j.apt.2017.10.023.
[52] I.O. Alade, M.A. Abd Rahman, T.A. Saleh, Predicting the specific heat capacity of alumina/ethylene glycol nanofluids using support vector regression model optimized with Bayesian algorithm, Sol. Energy. 183 (2019) 74–82, doi:10.1016/j.solener.2019.02.060.
[53] I.O. Alade, M.A. Abd Rahman, T.A. Saleh, Modeling and prediction of the specific heat capacity of Al2 O3/water nanofluids using hybrid genetic algorithm/support vector regression model, Nano-Structures & Nano-Objects. 17 (2019) 103–111, doi:10.1016/J.NANOSO.2018.12.001.
[54] I.O. Alade, M.A.A. Rahman, T.A. Saleh, An approach to predict the isobaric specific heat capacity of nitrides/ethylene glycol-based nanofluids using support vector regression, J. Energy Storage. 29 (2020) 101313, doi:10.1016/j.est.2020.101313.
[55] M. Mehrabi, M. Sharifpur, J.P. Meyer, Viscosity of nanofluids based on an artificial intelligence model, Int. Commun. Heat Mass Transf. 43 (2013) 16–21, doi:10.1016/j.icheatmasstransfer.2013.02.008.
[56] S. Khosrojerdi, M. Vakili, M. Yahyaei, K. Kalhor, Thermal conductivity modeling of graphene nanoplatelets/deionized water nanofluid by MLP neural network and theoretical modeling using experimental results, Int. Commun. Heat Mass Transf. 74 (2016) 11–17, doi:10.1016/j.icheatmasstransfer.2016.03.010.
[57] M. Gholizadeh, M. Jamei, I. Ahmadianfar, R. Pourrajab, Prediction of nanofluids viscosity using random forest (RF) approach, Chemom. Intell. Lab. Syst. 201 (2020) 104010, doi:10.1016/j.chemolab.2020.104010.
[58] M. Jamei, R. Pourrajab, I. Ahmadianfar, A. Noghrehabadi, Accurate prediction of thermal conductivity of ethylene glycol-based hybrid nanofluids using artificial intelligence techniques, Int. Commun. Heat Mass Transf. 116 (2020) 104624.
[59] I. Olanrewaju, M. Amiruddin, A. Rahman, Y. Yaakob, Application of support vector regression and artificial neural network for prediction of specific heat capacity of aqueous nano fluids of copper oxide, 197, 2020, pp. 485–490, doi:10.1016/j.solener.2019.12.067.
[60] I. Olanrewaju, M. Amiruddin, A. Rahman, A. Bagudu, Y. Yaakob, A. Saleh, Heliyon Development of a predictive model for estimating the specific heat capacity of metallic oxides/ethylene glycol-based nano fluids using support vector regression, 5, 2019, doi:10.1016/j.heliyon.2019.e01882.
[61] M.A. Hassan, D. Banerjee, A soft computing approach for estimating the specific heat capacity of molten salt-based nano fluids, J. Mol. Liq. 281 (2019) 365–375, doi:10.1016/j.molliq.2019.02.106.
[62] M. Jamei, I. Ahmadianfar, I.A. Olumegbon, M. Karbasi, A. Asadi, On the assessment of specific heat capacity of nanofluids for solar energy applications: Application of Gaussian process regression (GPR) approach, J. Energy Storage. 102067 (2020).
[63] S. Alotaibi, M.A. Amooie, M.H. Ahmadi, N. Nabipour, K. Chau, Modeling thermal conductivity of ethylene glycol-based nanofluids using multivariate adaptive regression splines and group method of data handling artificial neural network, Eng. Appl. Comput. Fluid Mech. 14 (2020) 379–390, doi:10.1080/19942060.2020.1715843.
[64] M.H. Ahmadi, B. Mohseni-Gharyehsafa, M. Farzaneh-Gord, R.D. Jilte, R. Kumar, K. Chau, Applicability of connectionist methods to predict dynamic viscosity of silver/water nanofluid by using ANN-MLP, MARS and MPR algorithms, Eng. Appl. Comput. Fluid Mech. 13 (2019) 220–228, doi:10.1080/19942060.2019.1571442.
[65] M.H. Ahmadi, B. Mohseni-Gharyehsafa, M. Ghazvini, M. Goodarzi, R.D. Jilte, R. Kumar, Comparing various machine learning approaches in modeling the dynamic viscosity of CuO/water nanofluid, J. Therm. Anal. Calorim. (2019), doi:10.1007/s10973-019-08762-z.
[66] M. Kahani, M. Ghazvini, B. Mohseni-Gharyehsafa, M.H. Ahmadi, A. Pourfarhang, M. Shokrgozar, S. Zeinali Heris, Application of M5 tree regression, MARS, and artificial neural network methods to predict the Nusselt number and output temperature of CuO based nanofluid flows in a car radiator, Int. Commun. Heat Mass Transf. 116 (2020) 104667, doi:10.1016/j.icheatmasstransfer.2020.104667.
[67] S. Yekani Motlagh, A. Sharifi, M. Ahmadi, H. Badfar, Presentation of new thermal conductivity expression for Al 2 O 3 –water and CuO –water nanofluids using gene expression programming (GEP), J. Therm. Anal. Calorim. 135 (2019) 195–206, doi:10.1007/s10973-018-7305-9.
[68] H.A. Al-Jamimi, T.A. Saleh, Transparent predictive modelling of catalytic hydrodesulfurization using an interval type-2 fuzzy logic, J. Clean. Prod. 231 (2019) 1079–1088, doi:10.1016/j.jclepro.2019.05.224.
[69] A. Mohebbi, Prediction of specific heat and thermal conductivity of nanofluids by a combined equilibrium and non-equilibrium molecular dynamics simulation, J. Mol. Liq. 175 (2012) 51–58, doi:10.1016/j.molliq.2012.08.010.
[70] G. Sadeghi, S. Nazari, M. Ameri, F. Shama, Energy and exergy evaluation of the evacuated tube solar collector using Cu2O/water nanofluid utilizing ANN methods, Sustain. Energy Technol. Assessments. 37 (2020) 100578, doi:10.1016/j.seta.2019.100578.
[71] H. Riazi, T. Murphy, G.B. Webber, R. Atkin, S.S.M. Tehrani, R.A. Taylor, Specific heat control of nanofluids: A critical review, Int. J. Therm. Sci. 107 (2016) 25–38, doi:10.1016/j.ijthermalsci.2016.03.024.
[72] I.M. Shahrul, I.M. Mahbubul, S.S. Khaleduzzaman, R. Saidur, M.F.M. Sabri, A comparative review on the specific heat of nanofluids for energy perspective, Renew. Sustain. Energy Rev. 38 (2014) 88–98, doi:10.1016/j.rser.2014.05.081.
[73] G. Huminic, A. Huminic, Application of nanofluids in heat exchangers: A review, Renew. Sustain. Energy Rev. 16 (2012) 5625–5638, doi:10.1016/j.rser.2012.05.023.
[74] H. Khodadadi, S. Aghakhani, H. Majd, R. Kalbasi, S. Wongwises, M. Afrand, A comprehensive review on rheological behavior of mono and hybrid nanofluids: Effective parameters and predictive correlations, Int. J. Heat Mass Transf. 127 (2018) 997–1012, doi:10.1016/j.ijheatmasstransfer.2018.07.103.
[75] M.A. Hassan, D. Banerjee, A soft computing approach for estimating the specific heat capacity of molten salt-based nanofluids, J. Mol. Liq. 281 (2019) 365–375, doi:10.1016/j.molliq.2019.02.106.
[76] J.M. Smith, Introduction to chemical engineering thermodynamics, J. Chem. Educ. 27 (1950) 584, doi:10.1021/ed027p584.3.
[77] J. Buongiorno, Convective transport in nanofluids, J. Heat Transfer. 128 (2006) 240–250, doi:10.1115/1.2150834.
[78] B.C. Pak, Y.I. Cho, Hydrodynamic and heat transfer study of dispersed fluids with submicron metallic oxide particles, Exp. Heat Transf. 11 (1998) 151–170, doi:10.1080/08916159808946559.
[79] S.U.S. Choi, S. Li, J.A. Eastman, Measuring thermal conductivity of fluids containing oxide nanoparticles, J. Heat Transfer. 121 (1999) 280–289, doi:10.1115/1.2825978.
[80] T.-P. Teng, Y.-H. Hung, Estimation and experimental study of the density and specific heat for alumina nanofluid, J. Exp. Nanosci. 9 (2014) 707–718, doi:10.1080/17458080.2012.696219.
[81] D. Cabaleiro, C. Gracia-Fernández, J.L. Legido, L. Lugo, Specific heat of metal oxide nanofluids at high concentrations for heat transfer, Int. J. Heat Mass Transf. 88 (2015) 872–879, doi:10.1016/j.ijheatmasstransfer.2015.04.107.
[82] Y.R. Sekhar, K.V. Sharma, Study of viscosity and specific heat capacity characteristics of water-based Al $_2$ O $_3$ nanofluids at low particle concentrations, J. Exp. Nanosci. 10 (2015) 86–102, doi:10.1080/17458080.2013.796595.
[83] R.S. Vajjha, D.K. Das, Specific heat measurement of three nanofluids and development of new correlations, J. Heat Transfer. 131 (2009) 1–7, doi:10.1115/1.3090813.
[84] B.X. Wang, L.P. Zhou, X.F. Peng, X.Z. Du, Y.P. Yang, On the specific heat capacity of CuO nanofluid, Adv. Mech. Eng. 2010 (2010), doi:10.1155/2010/172085.
[85] B. Barbés, R. Páramo, E. Blanco, M.J. Pastoriza-Gallego, M.M. Piñeiro, J.L. Legido, C. Casanova, Thermal conductivity and specific heat capacity measurements of Al 2O3 nanofluids, J. Therm. Anal. Calorim. 111 (2013) 1615–1625, doi:10.1007/s10973-012-2534-9.
[86] R.S. Vajjha, D.K. Das, Specific heat measurement of three nanofluids and development of new correlations, J. Heat Transfer. 131 (2009) 1–7, doi:10.1115/1.3090813.
[87] A.M. Hussein, R.A. Bakar, K. Kadirgama, K.V. Sharma, Experimental measurement of nanofluids thermal properties, Int. J. Automot. Mech. Eng. 7 (2013) 850–863, doi:10.15282/ijame.7.2012.5.0070.
[88] Y.I.C. Bock Choon Pak, Hydrodynamic and heat transfer study of dispersed fluids with submicron metallic oxide, Exp. Heat Transf. A J. , Therm. Energy Transp. , Storage , Convers. (2013) 37–41.
[89] S.M.S. Murshed, Determination of effective specific heat of nanofluids, J. Exp. Nanosci. 6 (2011) 539–546, doi:10.1080/17458080.2010.498838.
[90] I.M. Mahbubul, A. Saadah, R. Saidur, M.A. Khairul, A. Kamyar, Thermal performance analysis of Al2O3/R-134a nanorefrigerant, Int. J. Heat Mass Transf. 85 (2015) 1034–1040, doi:10.1016/j.ijheatmasstransfer.2015.02.038.
[91] H. O'Hanley, J. Buongiorno, T. McKrell, L.W. Hu, Measurement and model validation of nanofluid specific heat capacity with differential scanning calorimetry, Adv. Mech. Eng. 2012 (2012), doi:10.1155/2012/181079.
[92] J.R. Satti, D.K. Das, D. Ray, Specific heat measurements of five different propylene glycol based nanofluids and development of a new correlation, Int. J. Heat Mass Transf. 94 (2016) 343–353, doi:10.1016/j.ijheatmasstransfer.2015.11.065.
[93] B. Barbés, R. Páramo, E. Blanco, C. Casanova, Thermal conductivity and specific heat capacity measurements of CuO nanofluids, J. Therm. Anal. Calorim. 115 (2014) 1883–1891, doi:10.1007/s10973-013-3518-0.
[94] O.A. Alawi, A.R. Mallah, S.N. Kazi, M.N.M. Zubir, C.S. Oon, Thermal transport feasibility of (Water + Ethylene Glycol)-based nanofluids containing metallic oxides: mathematical approach, IOP Conf. Ser. Mater. Sci. Eng. 854 (2020), doi:10.1088/1757-899X/854/1/012023.
[95] S. Akilu, A.T. Baheta, K.V. Sharma, PT US, J. Mol. Liq. (2017), doi:10.1016/j.molliq.2017.09.017.
[96] Z.K. Kadhim, M.S. Kassim, A.Y. Abdul Hassan, Effect of (MGO) nanofluid on heat transfer characteristics for integral finned tube heat exchanger, Int. J. Mech. Eng. Technol. 7 (2016) 11–24.
[97] S. Choudhary, A. Sachdeva, P. Kumar, Investigation of the stability of MgO nanofluid and its effect on the thermal performance of flat plate solar collector, Renew. Energy. 147 (2020) 1801–1814, doi:10.1016/j.renene.2019.09.126.
[98] M. Jamei, I. Ahmadianfar, X. Chu, Z.M. Yaseen, Estimation of triangular side orifice discharge coefficient under a free flow condition using data-driven models, Flow Meas. Instrum. 101878 (2020).

[99] M. Kobayashi, S. Sakata, Mallows' Cp criterion and unbiasedness of model selection, J. Econom. 45 (1990) 385–395.
[100] N.M. Razali, Y.B. Wah, Power comparisons of shapiro-wilk, kolmogorov-smirnov, lilliefors and anderson-darling tests, J. Stat. Model. Anal. 2 (2011) 21–33.
[101] J. Quinlan, Learning with continuous classes, in: A. Adams, L. Sterling (Eds.), AI'92: Proceedings of the 5th Australian Joint Conference on Artificial Intelligence, 1992, pp. 343–348.
[102] A. Ghaemi, M. Rezaie-Balf, J. Adamowski, O. Kisi, J. Quilty, On the applicability of maximum overlap discrete wavelet transform integrated with MARS and M5 model tree for monthly pan evaporation prediction, Agric. For. Meteorol. 278 (2019) 107647.
[103] B. Keshtegar, C. Mert, O. Kisi, Comparison of four heuristic regression techniques in solar radiation modeling: Kriging method vs RSM, MARS and M5 model tree, Renew. Sustain. Energy Rev. 81 (2018) 330–341, doi:10.1016/j.rser.2017.07.054.
[104] M. Jamei, I. Ahmadianfar, Prediction of scour depth at piers with debris accumulation effects using linear genetic programming, Mar. Georesources Geotechnol. 38 (2020) 468–479.
[105] D. Alberg, M. Last, A. Kandel, Knowledge discovery in data streams with regression tree methods, Wiley Interdiscip. Rev. Data Min. Knowl. Discov. 2 (2012) 69–78.
[106] J.H. Friedman, Multivariate adaptive regression splines, Ann. Stat. (1991) 1–67.
[107] J.H. Friedman, C.B. Roosen, An introduction to multivariate adaptive regression splines, Stat. Methods Med. Res. 4 (1995) 197–217, doi:10.1177/096228029500400303.
[108] J. Adamowski, H.F. Chan, S.O. Prasher, V.N. Sharda, Comparison of multivariate adaptive regression splines with coupled wavelet transform artificial neural networks for runoff forecasting in Himalayan micro-watersheds with limited data, J. Hydroinformatics. 14 (2012) 731–744, doi:10.2166/hydro.2011.044.
[109] V.N. Sharda, S.O. Prasher, R.M. Patel, P.R. Ojasvi, C. Prakash, Performance of multivariate adaptive regression splines (MARS) in predicting runoff in mid-Himalayan micro-watersheds with limited data, Hydrol. Sci. J. 53 (2008) 1165–1175, doi:10.1623/hysj.53.6.1165.
[110] A. Mohanta, K.C. Patra, MARS for prediction of shear force and discharge in two-stage meandering channel, J. Irrig. Drain. Eng. 145 (2019) 1–17, doi:10.1061/(ASCE)IR.1943-4774.0001402.
[111] L. Wang, C. Wu, X. Gu, H. Liu, G. Mei, W. Zhang, Probabilistic stability analysis of earth dam slope under transient seepage using multivariate adaptive regression splines, 2020.
[112] G. Zheng, W. Zhang, H. Zhou, P. Yang, Multivariate adaptive regression splines model for prediction of the liquefaction-induced settlement of shallow foundations, Soil Dyn. Earthq. Eng. 132 (2020) 106097, doi:10.1016/j.soildyn.2020.106097.
[113] C. Ferreira, Gene expression programming: mathematical modeling by an artificial intelligence, Springer, 2006.
[114] A.H. Gandomi, A.H. Alavi, C. Ryan, Handbook of genetic programming applications, Springer, 2015.
[115] I. Ahmadianfar, M. Jamei, X. Chu, Prediction of local scour around circular piles under waves using a novel artificial intelligence approach, Mar. Georesources Geotechnol. (2019) 1–12.
[116] G. Lu, H. Huang, D. Zhang, Prediction of sweetpotato starch physiochemical quality and pasting properties using near-infrared reflectance spectroscopy, Food Chem. 94 (2006) 632–639, doi:10.1016/j.foodchem.2005.02.006.
[117] X. Su, J. An, Y. Zhang, P. Zhu, B. Zhu, Prediction of ozone hourly concentrations by support vector machine and kernel extreme learning machine using wavelet transformation and partial least squares methods, Atmos. Pollut. Res. 11 (6) (2020).
[118] Q. Fu, W. Shen, X. Wei, Y. Zhang, H. Xin, Z. Su, C. Zhao, Prediction of the diet energy digestion using kernel extreme learning machine: A case study with Holstein dry cows, Comput. Electron. Agric. 169 (2020) 105231.
[119] C.J. Willmott, Some Comments on the Evaluation of Model Performance, American Meteorological Society, 1982, doi:10.1175/1520-0477(1982)063<1309:SCOTEO>2.0.CO;2.
[120] D. Shin, D. Banerjee, Enhanced thermal properties of SiO2 nanocomposite for solar thermal energy storage applications, Int. J. Heat Mass Transf. 84 (2015) 898–902, doi:10.1016/j.ijheatmasstransfer.2015.01.100.
[121] S. Akilu, A.T. Baheta, K.V. Sharma, M.A. Said, Experimental determination of nanofluid specific heat with SiO2 nanoparticles in different base fluids, AIP Conf. Proc. 2017 (1877), doi:10.1063/1.4999896.
[122] Y. Xuan, W. Roetzel, Conceptions for heat transfer correlation of nanofluids, Int. J. Heat Mass Transf. 43 (2000) 3701–3707, doi:10.1016/S0017-9310(99)00369-5.
[123] R.S. Vajjha, D.K. Das, A review and analysis on influence of temperature and concentration of nanofluids on thermophysical properties, heat transfer and pumping power, Int. J. Heat Mass Transf. 55 (2012) 4063–4078, doi:10.1016/j.ijheatmasstransfer.2012.03.048.
[124] R. Pourrajab, I. Ahmadianfar, M. Jamei, M. Behbahani, A meticulous intelligent approach to predict thermal conductivity ratio of hybrid nanofluids for heat transfer applications, J. Therm. Anal. Calorim. (2020) 1–18.
[125] M. Jamei, I. Ahmadianfar, A rigorous model for prediction of viscosity of oil-based hybrid nanofluids, Phys. A Stat. Mech. Its Appl. 124827 (2020).
[126] J.R. Satti, D.K. Das, D. Ray, Specific heat measurements of five different propylene glycol based nanofluids and development of a new correlation, Int. J. Heat Mass Transf. 94 (2016) 343–353, doi:10.1016/j.ijheatmasstransfer.2015.11.065.
[127] W.-S. Han, S.-H. Rhi, Thermal characteristics of grooved heat pipe with hybrid nanofluids, Therm. Sci. 15 (2011) 195–206.
[128] L. Sang, T. Liu, The enhanced specific heat capacity of ternary carbonates nanofluids with different nanoparticles, Sol. Energy Mater. Sol. Cells. 169 (2017) 297–303.